Kim *et al. Nano Convergence* (2026) 13:7
https://doi.org/10.1186/s40580-026-00537-1

Nano Convergence

REVIEW Open Access

# Design strategies, methods, and photophysical insights in polymeric photocatalysts for solar-driven hydrogen evolution

Sowon Kim[1], Myungjin Kim[1], Danielle R. Lustig[2], Gayoung Ham[1], Changwoo Park[1], Damin Lee[1], Ludmilla Steier[2] and Hyojung Cha[1*]

**Abstract**

Solar-driven hydrogen evolution is emerging as a pivotal strategy in the sustainable energy transition, offering a viable pathway for renewable hydrogen production. Inorganic photocatalysts, such as metal oxides, sulfides, and carbon-based materials, have been extensively studied; however, their performance is often limited by poor tunability of energy levels and structures, low processability, and inadequate utilization of visible light. In contrast, polymeric photocatalysts offer distinct advantages, including precise molecular tunability, scalable fabrication *via* solution processing, and adjustable energy levels for optimized solar absorption. This review highlights recent advances in polymeric photocatalysts, with particular emphasis on molecular- and particle-level design strategies, fabrication methodologies, and photophysical insights. Molecular design approaches, such as backbone engineering, side-chain modification, and heteroatom incorporation, are discussed alongside particle-level optimization through control of size, morphology, and molecular ordering. Emerging fabrication techniques, including direct polymer dispersions and nanoparticle-based processing, are examined in relation to their effects on dispersibility, light harvesting, and catalytic activity. Photophysical studies are also emphasized to elucidate charge-carrier dynamics and to establish structure–property–performance correlations. Finally, evaluation methodologies, such as hydrogen evolution performance metrics, benchmarking practices, and ongoing challenges in standardization, are critically assessed. This review aims to synthesize current achievements and provide perspectives to guide future research toward the practical implementation of polymeric photocatalysts for solar-driven hydrogen evolution.

**Highlights**

- Recent progress in polymeric photocatalysts for solar hydrogen evolution is reviewed.
- Design, fabrication, and photophysical considerations are systematically discussed.
- Structure–property–performance relationships are emphasized.
- Key challenges and future perspectives in performance evaluation are outlined.

*Correspondence:
Hyojung Cha
hcha@knu.ac.kr

Full list of author information is available at the end of the article

**Keywords** Photocatalysis, Polymers, Hydrogen, Molecular design, Nanoparticle fabrication, Photophysics

**Graphical abstract**

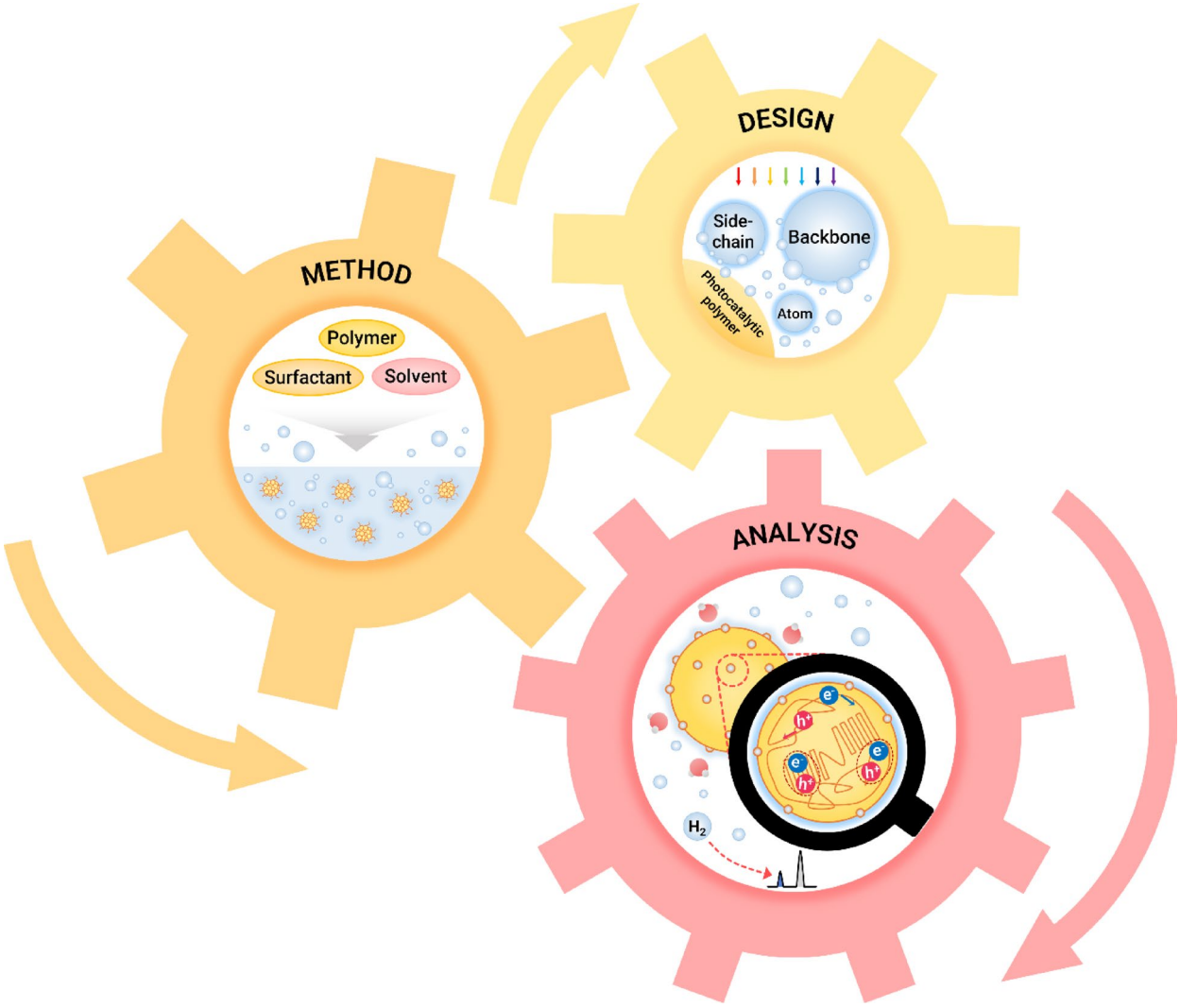


## 1 Introduction

The escalating global energy crisis and the urgent need to mitigate climate change have intensified international efforts to develop sustainable energy technologies [1]. Fossil fuels, which currently dominate the global energy supply, are finite and remain the primary contributors to greenhouse gas emissions, air pollution, and environmental degradation [2]. To meet the carbon neutrality targets set by many nations for the mid-21st century, a transition to renewable and carbon-free energy sources is imperative [3, 4]. Among various alternatives, solar energy is particularly promising due to its unmatched abundance and inexhaustibility [5]. However, the efficient capture and storage of solar energy in a practical, usable form continues to pose significant scientific and technological challenges [6]. In this context, direct solar-to-chemical conversion, wherein solar photons are harnessed to drive chemical reactions, has emerged as an especially attractive approach. Three primary strategies have been proposed for solar hydrogen production: photovoltaic (PV)-driven electrolysis, photoelectrochemical (PEC) water splitting, and photocatalysis (Fig. 1). The latter is by far the least efficient, but it also offers a simpler and potentially more cost-effective system [7–11]. In PV-driven electrolysis, hydrogen is generated by first producing electricity via solar cells, which is then used to split water into hydrogen and oxygen (Fig. 1a). This method benefits from the high efficiency of mature photovoltaic technologies; however, it necessitates separate components, including solar modules, electrolyzers, and

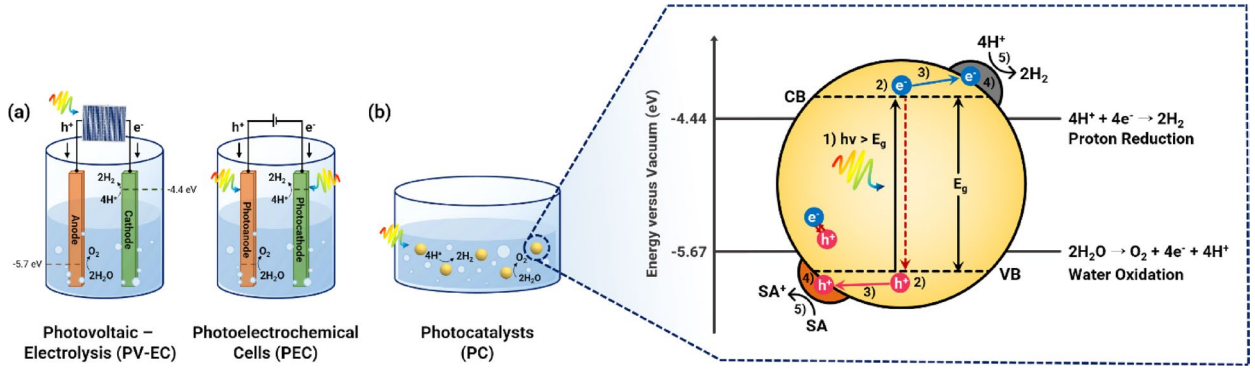


**Fig. 1** **a** Schematic illustration of a solar-driven hydrogen evolution system and **b** the operating mechanism of photocatalysts: (1) absorption of photons with energies exceeding the bandgap, (2) exciton generation and dissociation, (3) charge transport and extraction, (4) charge accumulation, and (5) the hydrogen-evolution reaction

external power management systems, which increases system complexity and capital costs [12, 13]. By contrast, PEC water splitting integrates light absorption and electrochemical conversion within a single device, offering a more compact and potentially cost-effective solution (Fig. 1a) [14, 15]. In PEC systems, photoelectrodes directly harvest sunlight to drive water splitting and, in some cases, can operate without an external bias [16]. This configuration offers relatively high energy conversion efficiency and a simplified device architecture. However, practical implementation is constrained by several challenges, including limited long-term stability of photoelectrodes and difficulties in fabricating polymer-based photocathodes or anodes, particularly delamination of the polymer film from the substrate [16–18]. Among the three strategies, photocatalytic water splitting represents the most straightforward approach, enabling direct hydrogen generation from water using only light, without the need for an external electrical bias (Fig. 1b). Owing to the ability to disperse photocatalysts in solution or process them into films and coatings, this method is well-suited for scalable reactor configurations [19]. The combination of conceptual simplicity, low material cost, and compatibility with large-area systems positions photocatalysis as a promising platform for solar fuel production. In particular, solar-driven photocatalytic hydrogen evolution offers an environmentally benign route to produce hydrogen, a clean fuel with high gravimetric energy density, by utilizing water and sunlight as abundant, renewable resources [20, 21].

Nevertheless, translating these advantages into practical and efficient systems remains a significant challenge. Despite decades of progress, the field of photocatalytic hydrogen evolution continues to face formidable obstacles. Effective photocatalysts must simultaneously exhibit broad and strong light absorption, rapid generation of charge carriers, efficient separation and transport of electrons and holes, and robust catalytic sites to drive the hydrogen evolution reaction [22, 23]. Achieving all these properties within a single material has proven difficult; therefore, the rational and predictive design of photocatalysts remains a central focus of ongoing research [24, 25].

Inorganic photocatalysts, such as metal oxides, metal sulfides, and carbon-based semiconductors, have been extensively studied, providing a solid foundation for understanding the fundamental principles of photocatalysis (Fig. 2a) [26–28]. Seminal studies include $TiO_2$-based systems reported by Fujishima and Honda for overall water splitting, visible-light-driven hydrogen evolution using CdS and ZnS sulfides, and the development of graphitic carbon nitride (g-$C_3N_4$) as a metal-free photocatalyst [29–32]. However, these materials suffer from several intrinsic limitations. Their electronic structures and bandgaps are often difficult to tune, which constrains the optimization of energy level alignment with water redox potentials [33, 34]. In addition, many inorganic photocatalysts display poor solution processability, require high-temperature synthesis, and offer limited structural flexibility, all of which hinder large-scale fabrication and integration into functional devices [35–37].

Polymeric photocatalysts have recently emerged as a promising class of materials to overcome the limitations of inorganic systems (Fig. 2a, b). Leveraging the vast design space of organic chemistry, polymer backbones and side chains can be synthetically tailored to modulate electronic and optical properties, charge carrier dynamics, and molecular packing, thereby enabling performance enhancements that are often difficult to achieve with conventional inorganic semiconductors [38–40]. Early studies demonstrated that simple aromatic polymers, such as poly(p-phenylene) and poly(p-phenylene vinylene), could evolve hydrogen under sacrificial conditions, establishing the fundamental feasibility of organic photocatalysis [41, 42]. Subsequent developments introduced heteroatom-containing frameworks, including the

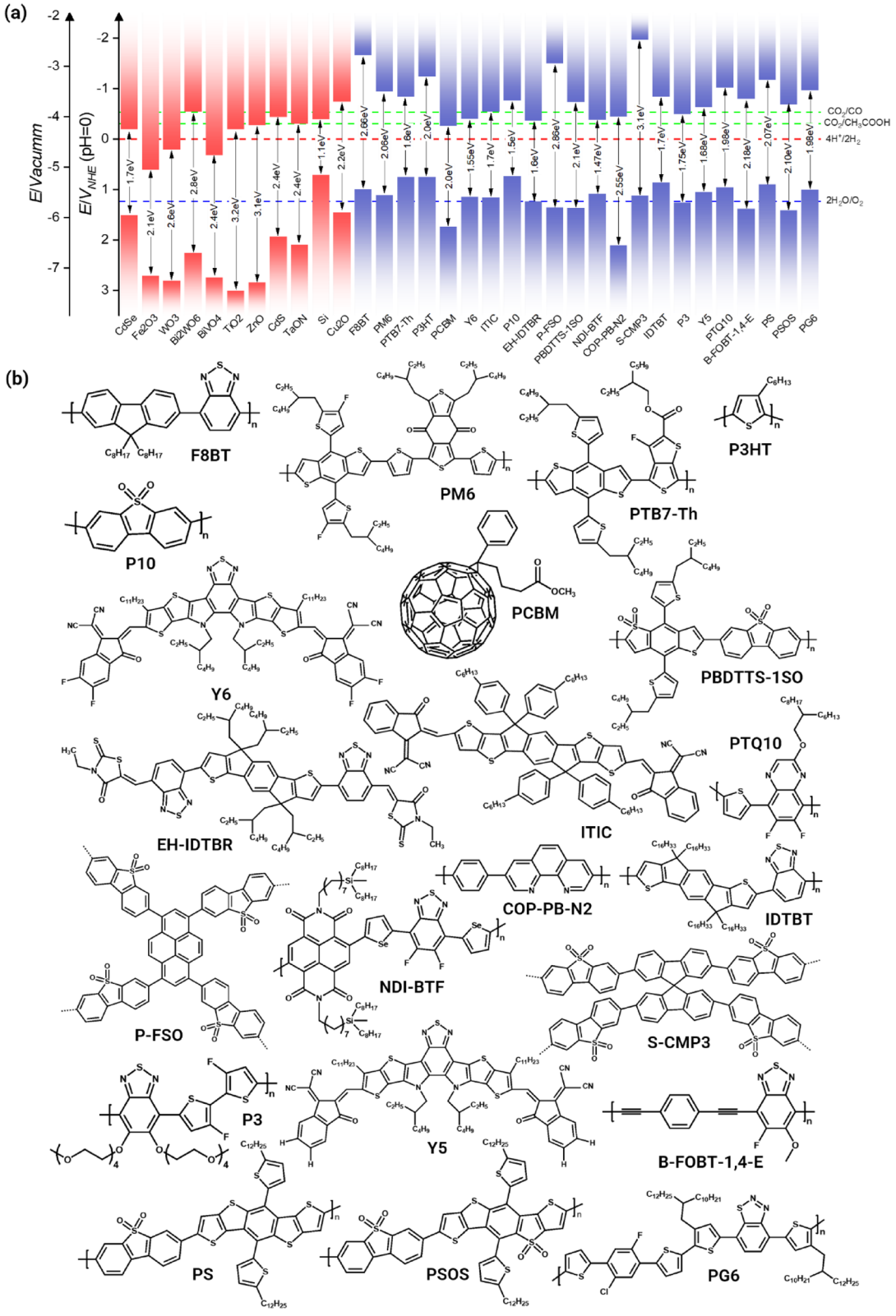


**Fig. 2** **a** Energy levels of inorganic and organic materials, and **b** representative organic molecules and polymer structures employed as photocatalyst materials

dibenzo[b, d]thiophene sulfone (DBS)-based polymer P10, which exhibited significantly improved hydrogen evolution performance [43, 44]. This enhancement was attributed primarily to the presence of highly polar sulfone groups that strengthen polymer–water interactions, thereby facilitating proton access and interfacial charge transfer [43]. Beyond P10, conjugated polymers such as poly(9,9-dioctylfluorene-alt-benzothiadiazole) (F8BT) and related benzothiadiazole (BT) derivatives have also demonstrated enhanced photocatalytic activity [45, 46]. In these systems, the nitrogen atoms in the BT units are believed to act as proton-binding sites, promoting proton reduction at the polymer–water interface [47, 48]. More recently, binary and ternary polymeric systems have been developed to combine complementary absorption profiles and establish cascade energy-level alignment, enabling broader spectral utilization and more efficient charge separation [49–51].

However, polymeric systems also present distinct scientific challenges (Fig. 3a). Unlike inorganic semiconductors, organic conjugated polymers possess intrinsically low dielectric constants ($\varepsilon_r$), which enhance Coulombic attraction between electrons and holes, resulting in tightly bound Frenkel-type excitons with small Bohr radii, significantly limiting the generation of free charge carriers [52, 53]. Furthermore, many polymer photocatalysts exhibit amorphous or weakly crystalline morphologies, which restrict charge transport pathways and hinder interfacial charge transfer [12]. In addition, polymer photocatalysts synthesized via coupling reactions often contain trace metal impurities, which can act as unintended co-catalysts or charge recombination centers, complicating the interpretation of intrinsic photocatalytic activity [54, 55]. These intrinsic limitations, coupled with generally modest charge carrier mobilities, contribute to the overall inefficiency of photocatalytic performance. As a result, many reported polymer photocatalysts still demonstrate relatively moderate hydrogen evolution rates (HERs) compared to benchmark inorganic systems, highlighting the continued need for improved molecular design, enhanced morphological control, and deeper mechanistic insight into structure–property–performance relationships (Fig. 3b–d) [56–59].

To address these challenges, recent studies have combined innovative processing techniques with advanced structural analyses to elucidate how molecular organization and morphology influence photocatalytic performance. One such technique involves the direct dispersion of polymers in solvent systems, where the extent of polymer–solvent interactions, dictated by molecular design, significantly affects structural organization and photophysical properties [60–62]. Another promising strategy is the fabrication of polymer nanoparticles, which effectively mitigates issues related to limited charge transport and poor dispersibility. By tuning particle size, morphology, and surface chemistry, these nanoparticle formulations enhance both stability and accessible surface area while improving interactions with the aqueous environment and promoting more efficient charge separation and transport [63–65]. As a result, particle-level engineering is becoming essential for translating the intrinsic advantages of polymers into high-performance photocatalysts.

In parallel, photophysical investigations have provided critical insights into the structure–property–performance relationships of polymeric photocatalysts [12, 43, 66]. Advanced spectroscopic techniques, including

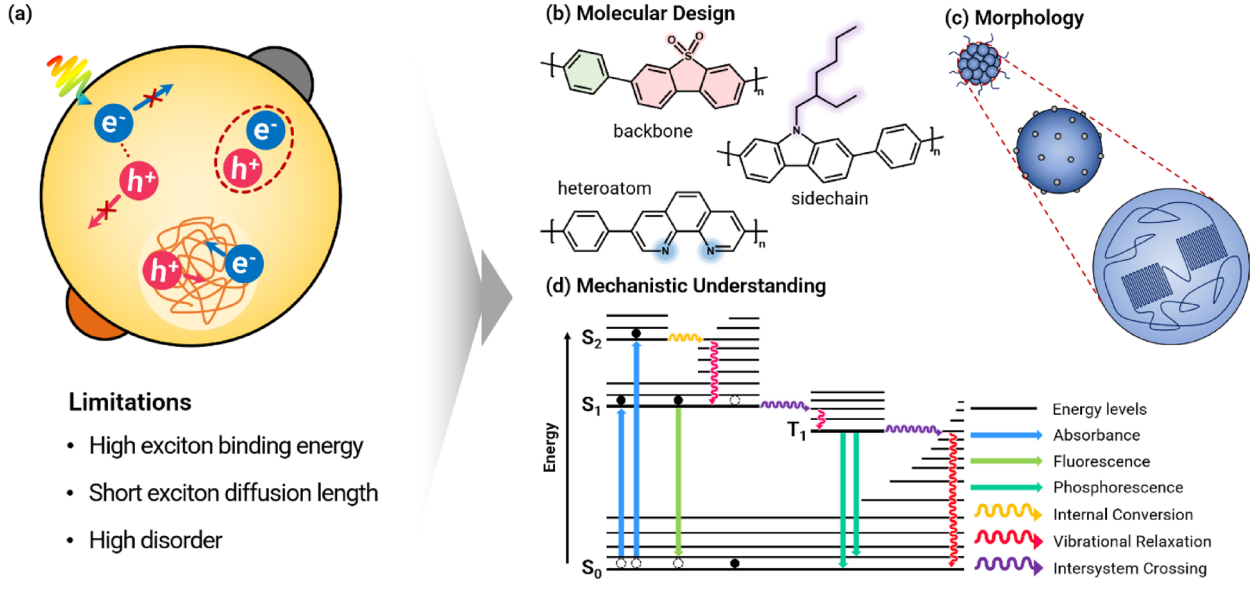


**Fig. 3** **a** Intrinsic limitations of organic materials for photocatalysis and corresponding strategies to overcome them, including approaches based on **b** molecular design, **c** morphology control, and **d** mechanistic understanding

time-resolved photoluminescence (Tr-PL), transient absorption spectroscopy (TAS), and photoinduced absorption spectroscopy (PIAS), have elucidated the fundamental dynamics of charge carriers, underscoring the decisive influence of structural and molecular features on charge separation and transport [12, 67]. Establishing robust correlations between photophysical behavior and material design strategies is therefore essential for developing a more rational, mechanism-guided framework for polymeric photocatalyst development. Nevertheless, there remains a pressing need for comprehensive reviews that encompass the full research workflow of polymeric photocatalysts, from synthesis and molecular design to particle engineering, photophysical characterization, and performance evaluation, in order to construct a holistic framework for the field.

Accordingly, the aim of this review is to present a comprehensive and integrated perspective on the design strategies, fabrication methods, photophysical mechanisms, and performance of polymeric photocatalysts for solar-driven hydrogen evolution. We begin by summarizing molecular- and particle-level design strategies that have been employed to enhance photocatalytic performance, with a focus on molecular engineering approaches such as side-chain modification and heteroatom incorporation. This is followed by a discussion of fabrication methodologies, ranging from direct polymer dispersion to nanoparticle engineering, with emphasis on their structural properties and catalytic activity. We then examine recent spectroscopic studies to connect charge carrier dynamics with structural and morphological parameters. Finally, we identify key challenges and knowledge gaps that must be addressed to fully realize the potential of polymeric photocatalysts and outline future research directions to accelerate their development. Through this integrated approach, we aim to provide a roadmap for both materials design and mechanistic understanding, thereby advancing the field toward practical solar-to-hydrogen conversion.

## 2 Molecular and particle design strategies

Molecular and particle design strategies form the foundation for optimizing the performance of polymeric photocatalysts. Backbone engineering, side-chain modification, and heteroatom incorporation allow precise control over intrinsic material properties, while tuning particle size and morphology influences colloidal stability and interfacial interactions. Together, these approaches regulate light absorption, charge separation, and interfacial catalysis. This section highlights key advances in these strategies and their impact on photocatalytic hydrogen evolution.

### 2.1 Molecular-level strategies

#### *2.1.1 Backbone engineering of polymers*

A fundamental strategy for enhancing polymeric photocatalysts is the rational design of the polymer backbone (Fig. 4a). Copolymers are often favored over homopolymers due to their greater structural tunability; by combining distinct monomeric units, copolymerization enables

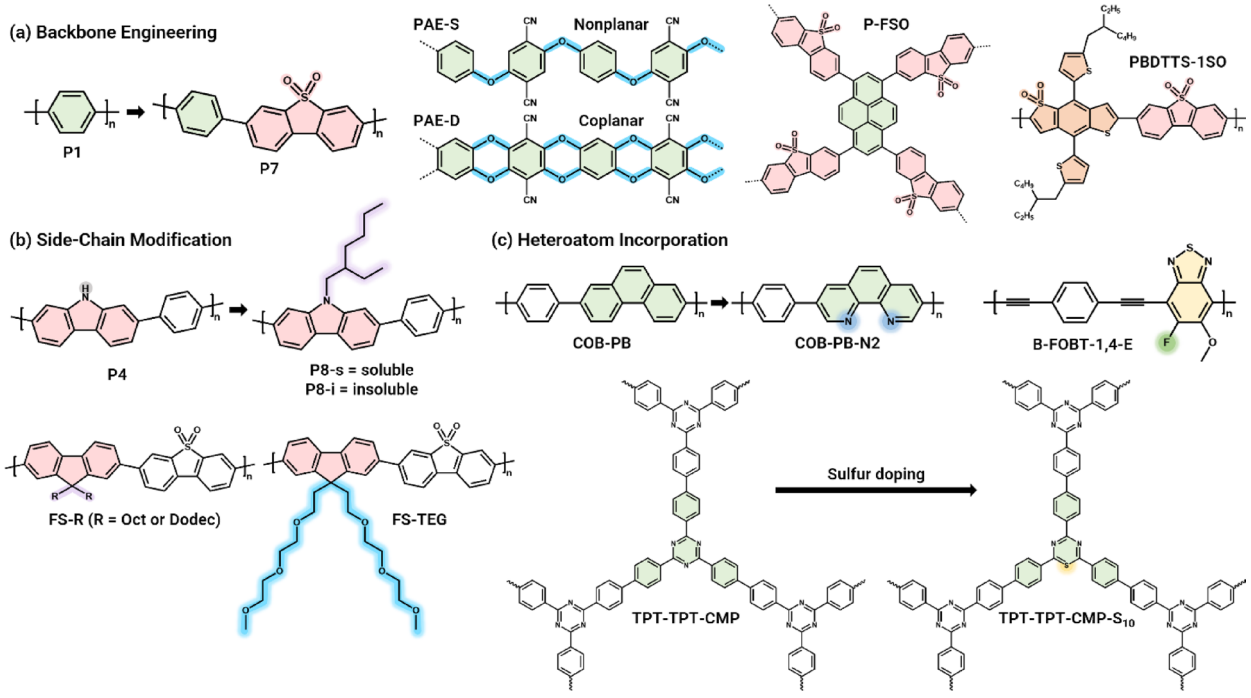


**Fig. 4** Polymer design strategies for photocatalysts: **a** backbone engineering, **b** side-chain modification, and **c** heteroatom incorporation

precise control over critical parameters such as electronic distribution, solubility, hydrophilicity, and molecular packing [68, 69]. Representative studies are discussed below to illustrate how backbone engineering influences photocatalytic performance. A notable example of copolymer-based design was reported by Sprick et al., who demonstrated that incorporating electron-deficient and planar units into poly(p-phenylene) (PPP), denoted as P1, significantly improved photocatalytic activity [70]. Copolymerization with motifs such as fluorene, carbazole, DBT, or DBS enhanced molecular planarity, broadened UV–visible light absorption and produced an optimal optical bandgap for proton reduction. As a result, the PPP–DBS copolymer P7 exhibited a substantially higher HER of 0.2 mmol $h^{-1}$, compared to its homopolymer counterparts, thereby underscoring copolymerization as an effective approach to tune both molecular planarity and optical properties. Building on this concept, one of the most widely adopted molecular design strategies in copolymer-based systems is the implementation of donor–acceptor (D–A) architectures. Alternating electron-rich and electron-deficient units enable modulation of the highest occupied molecular orbital (HOMO) and lowest unoccupied molecular orbital (LUMO) energy levels through intramolecular charge transfer, thereby tuning the bandgap to broaden visible-light absorption and align energy levels with water redox potentials [71]. In addition to bandgap control, D–A frameworks also affect charge dynamics; the built-in electric fields within the polymer backbone facilitate exciton dissociation and charge separation while suppressing charge recombination [72]. A notable example was reported by Lan et al., who designed a series of pyrene-based D–A copolymers incorporating dibenzothiophene-S, S-dioxide (FSO) units as electron-deficient acceptor moieties [73]. Incorporation of the FSO unit not only enhanced intramolecular charge transfer but also introduced an "electron-output tentacle," a localized sulfonyl oxygen site capable of efficiently transferring electrons to protons or residual Pd co-catalysts. Systematic substitution of benzene units with FSO progressively lowered the LUMO level, promoted exciton separation, and significantly increased the HER, even in the absence of additional metal co-catalysts. Through this molecular engineering strategy, the optimized copolymer P-FSO achieved a HER of 0.4 mmol $h^{-1}$, demonstrating the pivotal role of FSO units in facilitating efficient electron extraction and transfer. Furthermore, Lan et al. developed fully coplanar D–A polymers in which a rigid, double-linked structure between donor and acceptor units enforced backbone planarity [74]. This enhanced planarity strengthened charge transfer, narrowed the bandgap, and promoted exciton dissociation, resulting in substantial improvements in HER. The coplanar polymer PAE-D consequently achieved a significantly higher HER of 0.2 mmol $h^{-1}$, and an apparent quantum yield (AQY) of 5.6% at 420 nm, outperforming its non-planar analogue and demonstrating that backbone planarity is a critical design parameter alongside D–A pairing. More advanced strategies, such as dual-acceptor engineering, have further increased electron-withdrawing strength and improved the efficiency of electron extraction sites [75, 76]. A representative example is the work by Lin et al., who introduced a backbone-centered molecular engineering approach by oxidizing the 4,8-bis(5-(2-ethylhexyl)thiophen-2-yl)benzo[1,2-b:4,5-b′]dithiophene (BDTT) donor core to BDTT-nSO ($n$ = 1–4, indicating the number of sulfone groups, and copolymerizing these oxidized monomers with a dibenzo[b, d]thiophene-5,5-dioxide (S)-based acceptor to yield PBDTTS-nSO polymers [77]. This sulfide-to-sulfone backbone oxidation increased the density of sulfone electron-output sites and enhanced hydrophilicity, while the dual-acceptor ($A_1$–$A_2$) architecture facilitated more favorable charge separation. Among the series, PBDTTS-1SO exhibited the optimal balance of these attributes, achieving a HER of 97.1 mmol $g^{-1}$ $h^{-1}$ and an AQY of 18.5% at 500 nm. These results underscore that tailoring the conjugated backbone itself, beyond side-chain or acceptor-unit modification, represents a powerful design strategy for enhancing the photocatalytic efficiency of polymeric systems. As another example, Mekhemer et al. reported a dual-acceptor naphthalene diimide (NDI)-based polymer system, in which NDI serves as the primary acceptor ($A_1$), while an additional benzothiadiazole- or benzotriazole-based unit (BTF or BTzF) is directly incorporated into the π-conjugated backbone to form $A_1$–D–$A_2$ (or $A_3$)–D architectures [78]. This acceptor-enriched backbone facilitates directional electron transfer toward the NDI core, enhances charge separation, and, when formulated as PS–PEG–COOH polymer dots (Pdots), yields well-dispersed particles in water that enable visible-light-driven hydrogen evolution without the use of organic co-solvents. Notably, NDI-BTF–PS–PEG–COOH Pdots achieved a HER of 3.5 mmol $g^{-1}$ $h^{-1}$ and exhibited stable activity over 72 h, demonstrating that dual-acceptor backbone design is an effective strategy for enhancing both charge extraction and photocatalytic stability. These findings reinforce that careful backbone engineering enables the design of polymers with broad absorption profiles, efficient exciton dissociation, favorable charge transport, and well-aligned frontier orbital energies conducive to high photocatalytic activity.

#### *2.1.2 Side-chain modification*

Beyond the polymer backbone, side-chain engineering offers versatile opportunities to modulate key parameters such as solubility, morphology, and interfacial compatibility (Fig. 4b). Flexible alkyl side chains typically

enhance solubility in organic solvents, thereby enabling facile solution processing [79]. Representative examples are discussed to highlight the role of side-chain engineering in tuning solubility and processability. For example, Woods et al. introduced branched 2-ethylhexyl chains into an originally insoluble carbazole–phenylene polymer (P4), yielding a new material, P8, which could be separated into a chloroform-soluble fraction (P8-s) and an insoluble fraction (P8-i) [80]. This modification markedly improved solubility and enabled solution processing: P8-s could be cast into thin films, while P8-i preserved the bulk-like properties of the parent polymer. Notably, P8-i retained a HER of 0.9 mmol $g^{-1}$ $h^{-1}$, closely matching the activity of the unmodified polymer, while even the soluble fraction, P8-s, achieved a comparable HER of 0.5 mmol $g^{-1}$ $h^{-1}$. These results demonstrate that side-chain engineering can impart solution processability and thin-film fabricability without substantially compromising photocatalytic activity. More broadly, the study shows that tailoring alkyl side chains is an effective strategy to tune wettability, dispersibility, and scalability of polymer photocatalysts while largely preserving the intrinsic optoelectronic properties of the conjugated backbone. More recently, polar or hydrophilic side chains, such as oligo(ethylene glycol) units, have been incorporated to enhance polymer dispersibility in aqueous systems and strengthen polymer–water interactions [81]. In one example, Woods et al. modified a fluorene-based polymer by introducing oligo(ethylene glycol) side chains (FS-TEG), which significantly improved water wettability and polymer–water interactions compared to its alkyl-substituted analogue [82]. This hydrophilic environment enabled enhanced polymer swelling and resulted in a higher density and extended lifetime of electron polarons, while maintaining a similar optical bandgap and frontier orbital energy levels. As a result, FS-TEG achieved a HER of 2.9 mmol $g^{-1}$ $h^{-1}$, nearly double that of its hydrophobic counterpart. This case highlights how incorporating hydrophilic side chains can simultaneously improve water compatibility, increase the population and lifetime of photogenerated charges, and thereby enhance overall photocatalytic efficiency. Hence, side-chain engineering has become an essential tool for bridging molecular design with practical photocatalytic performance.

#### *2.1.3 Heteroatom incorporation*

Incorporating heteroatoms into the polymer backbone or side chains represents another powerful molecular-level strategy for modulating photocatalytic properties (Fig. 4c). Nitrogen, sulfur, and fluorine are commonly introduced due to their ability to adjust electron density, alter hydrogen bonding or dipole interactions, and introduce catalytically active sites [83]. For example, nitrogen incorporation can introduce proton-binding sites that serve as additional active centers for proton reduction, while sulfur atoms can extend π-conjugation and reduce the bandgap, thereby enhancing light harvesting and charge transfer efficiency [84]. This strategy is exemplified by Liu et al., who incorporated pyridinic nitrogen into a phenanthrene-based conjugated polymer (COP-PB), generating electron-rich active sites along the backbone. The nitrogen doping reduced the Gibbs free energy for proton adsorption, promoted charge localization at the nitrogen sites, and resulted in a five-fold increase in HER, from 0.01 to 0.05 mmol $h^{-1}$, in the nitrogen-enriched analogue COP-PB-N2 compared to the undoped COP-PB. Similarly, Elewa et al. demonstrated that sulfur doping in triazine-based conjugated microporous polymers (CMPs), achieved by partially substituting nitrogen with sulfur to form C–S bonds, narrowed the bandgap, extended visible-light absorption, and suppressed charge recombination [85]. Although the initial HER of the sulfur-doped polymer (TPT-TPT-CMP-$S_{10}$) slightly decreased relative to the undoped CMP, the doped samples exhibited significantly improved long-term stability, sustaining hydrogen evolution over 30–100 h without deactivation. This indicates that sulfur incorporation enhances photocatalytic durability and charge utilization over extended periods. Fluorination has also proven effective in lowering the activation barrier for hydrogen formation, enhancing charge mobility, and facilitating proton-coupled electron transfer (PCET) [86]. In a representative study, Xiang et al. developed a series of BT-based polymers with stepwise fluorination on the acceptor unit [86]. Increasing fluorine content enhanced the electron-withdrawing character, downshifted frontier orbital levels, and promoted PCET on the BT acceptor. As a result, the optimally fluorinated polymer achieved a HER of 0.4 mmol $h^{-1}$, approximately three times higher than its non-fluorinated analogue, along with an AQY of 5.7% at 420 nm. These heteroatom-based strategies underscore the versatility of organic synthesis in precisely tuning the optoelectronic and morphological characteristics of polymer photocatalysts.

### 2.2 Particle-level optimization

#### *2.2.1 Particle size control*

The control of particle size plays a decisive role in determining photocatalytic activity (Fig. 5a). Nanoscale particles offer a high surface-to-volume ratio, increasing the number of accessible catalytic sites and facilitating interfacial charge transfer [87]. As particle size increases, however, light absorption and charge transport within polymer particles can become spatially heterogeneous. In particular, larger particles may contain so-called dead zones, where photogenerated excitons or charge carriers fail to reach the particle–solution interface within their diffusion length, leading to increased bulk recombination [87]. In addition, optical loss can become more

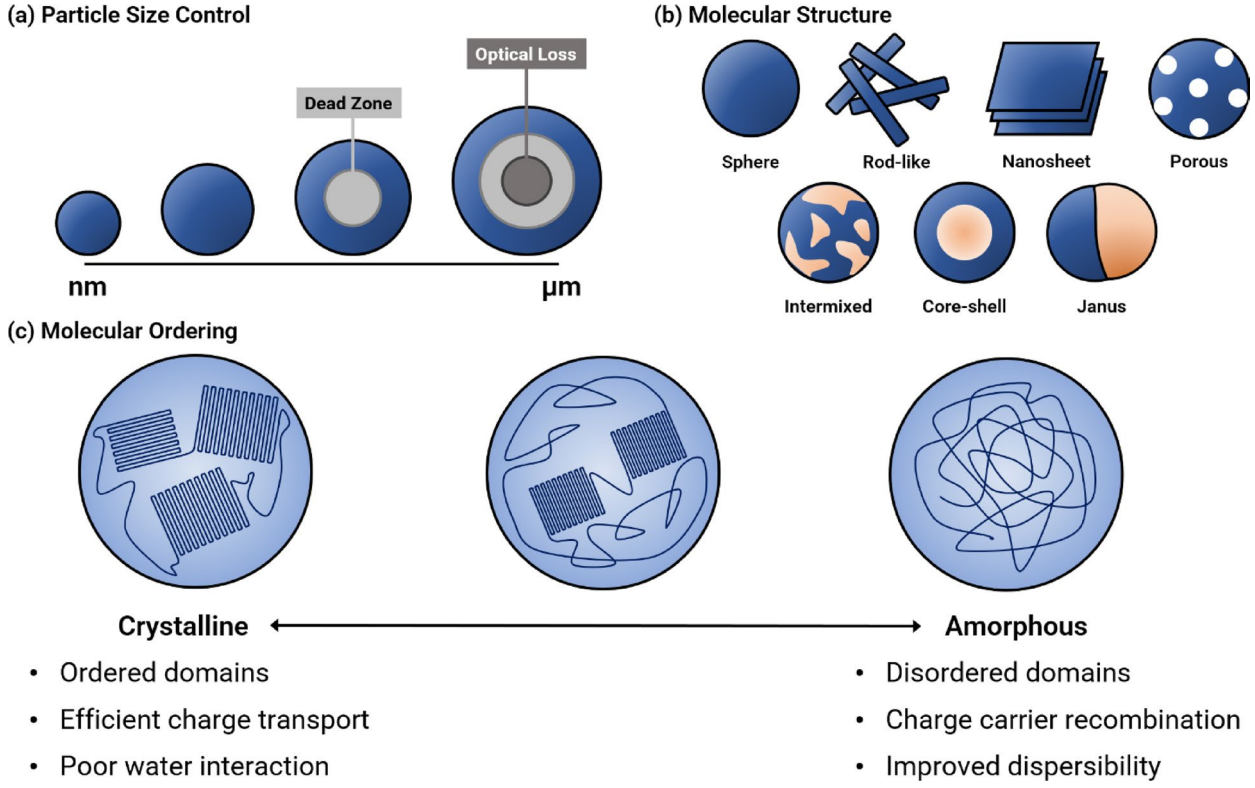


**Fig. 5** Understanding morphological approaches in polymer photocatalysts, including **a** particle size control, **b** molecular structure, and **c** molecular ordering within the particles

pronounced in larger particles due to enhanced light scattering and self-absorption, reducing the fraction of incident photons that effectively contribute to photocatalytic reactions [88]. These phenomena reflect size-dependent light–matter interactions and charge transport characteristics in polymeric photocatalysts, underscoring the importance of considering particle dimensions together with internal structure and accessibility. On this basis, reducing polymer particles to the nanoscale has been actively investigated. For instance, Aitchison et al. demonstrated that converting the microscale conjugated polymer P10 into nanoparticles (P10-e) via mini-emulsion polymerization significantly enhanced hydrogen evolution performance [89]. Reducing the particle size from the micrometer to approximately 150 nm improved water dispersibility and light scattering, while also shortening charge migration distances relative to the exciton diffusion length, thereby suppressing bulk recombination. As a result, P10-e nanoparticles achieved a HER of 60.6 mmol $g^{-1}$ $h^{-1}$ under visible light. Furthermore, this activity increased to 84.0 mmol $g^{-1}$ $h^{-1}$ following in situ photodeposition of 3 wt% Pt onto the material.

Beyond simple size reduction, particle size effects in polymeric photocatalysts should be considered together with internal surface area and accessibility. In this context, microscale polymer particles are frequently associated with porous polymer structures, where internal porosity significantly increases the interfacial area with water, thereby enhancing hydrogen evolution efficiency [90]. CMPs represent a representative class of materials in which the influence of particle size is effectively decoupled from surface accessibility owing to their intrinsic microporosity, highlighting the interplay between particle dimensions and internal surface area [91]. This concept is exemplified by recent studies on CMP-based photocatalysts. Sprick et al. showed that fluorene- and DBS-based CMPs (S-CMPs) can achieve high hydrogen evolution rates despite their micrometer-scale particle sizes, owing to their intrinsic microporosity and strong water uptake, particularly in S-CMP3 [90]. Notably, S-CMP3 exhibited a HER of 3.1 mmol $g^{-1}$ $h^{-1}$ under visible light and an AQY of 13.2% at 420 nm, outperforming its nonporous linear analogue. This indicates that internal pore networks, enhanced wettability, and pore accessibility can compensate for limited external surface area, enabling efficient charge separation and proton reduction within the internal pore network.

#### *2.2.2 Particle structure engineering*

Beyond particle size, particle structure plays a critical role in determining photocatalytic behavior (Fig. 5b). Spherical particles typically enable isotropic charge diffusion

and uniform dispersion, whereas anisotropic morphologies such as rods facilitate directional charge transport along preferred pathways [92, 93]. Porous architectures, defined by internal cavities and channels, offer enlarged surface areas and induce multiple scattering effects that enhance light absorption and water accessibility [94]. In systems composed of single or multiple polymers, cooperative packing and interfacial organization can produce complex morphologies, such as core–shell, Janus, or intermixed domains, which introduce additional interfaces that promote efficient light harvesting and charge separation [95]. A representative example is the PM6-based heterojunction system reported by Kosco et al., in which particle morphology is dictated by D–A miscibility [96]. PM6:Y6 forms an intermixed structure with randomly distributed semicrystalline domains, while the low miscibility between PM6 and PCBM results in a core–shell morphology, featuring a PCBM-rich core and a thin PM6 shell. This structural distinction significantly affects charge behavior: the core–shell PM6:PCBM nanoparticles enable more efficient interfacial charge separation and reduced recombination, leading to a higher HER (0.011 mmol $h^{-1}$ $m^{-2}$) compared to the intermixed PM6:Y6 system (0.010 mmol $h^{-1}$ $m^{-2}$). Overall, tailoring particle structure in both single-component and composite polymer systems has emerged as a versatile strategy to optimize light absorption, charge carrier dynamics, and hydrogen evolution performance.

#### *2.2.3 Molecular ordering within particles*

The degree of molecular ordering within polymer particles is a critical factor influencing photocatalytic performance (Fig. 5c). Ordered domains facilitate exciton transport and enhance charge-carrier mobility, whereas amorphous regions, though typically associated with higher recombination losses, can improve dispersibility and surface accessibility in aqueous media [97, 98]. Therefore, achieving an optimal balance between ordered and disordered domains is essential to simultaneously promote charge transport, exciton dissociation, and catalytic interface accessibility. For instance, Wang et al. demonstrated that introducing semicrystallinity into heptazine-based melon generates abundant order–disorder interfaces, which accelerate exciton dissociation and increase the population of free charge carriers [99]. In these semicrystalline particles, ordered domains support directional electron transport, while disordered regions serve as hole-blocking sites that suppress recombination. This structural modulation resulted in a sevenfold increase in electron concentration relative to the fully amorphous polymer, thereby enhancing electron-involved photocatalytic reactions. This case underscores that photocatalytic performance is governed not by crystallinity alone, but by the spatial integration of ordered and disordered domains within the polymer matrix. Similarly, Yang et al. designed ternary PM6:ITCC-M:IDMIC-4F nanoparticles, in which two structurally compatible ITIC-derived n-type molecules formed a compact alloy-like phase with shortened lattice spacing (~ 0.33 nm), thereby enhancing molecular ordering and charge-transfer efficiency [100]. This compact phase facilitated efficient exciton dissociation (97% photoluminescence quenching, 0.69 ns lifetime) and accelerated charge transport, achieving a remarkable HER of 307.0 mmol $g^{-1}$ $h^{-1}$ with an AQY of 5.9% at 600 nm, surpassing the binary PM6:ITCC-M system (260.0 mmol $g^{-1}$ $h^{-1}$). Additionally, the improved intermolecular packing enhanced structural stability, allowing retention of 81% of the initial activity after 40 h. This example highlights that controlled molecular ordering within nanoparticles is pivotal not only for maximizing photocatalytic efficiency but also for improving long-term operational stability.

## 3 Fabrication methods for polymeric photocatalysts

In addition to molecular design, the processing of polymers into functional photocatalysts plays a decisive role in determining their performance. Various fabrication strategies have been developed to optimize key parameters such as particle size, morphology, and stability, thereby enhancing light harvesting, charge separation, and catalytic activity. This section reviews two representative approaches, direct polymer dispersion and nanoparticle fabrication, highlighting their principles, advantages, and recent advances in the context of photocatalytic hydrogen evolution.

### 3.1 Direct polymer dispersion

One of the simplest methods for evaluating polymeric photocatalysts involves the direct dispersion of pristine polymers in photocatalytic solvents (Fig. 6a; Table 1). In this approach, polymer powders are introduced into mixed solvent systems, such as triethylamine (TEA)/methanol (MeOH)/water, where photocatalytic hydrogen evolution is directly assessed under light irradiation [43, 70, 73]. This method offers the advantage of simplicity, requiring minimal processing steps while enabling rapid evaluation of photocatalytic activity.

However, direct dispersion presents several drawbacks. Most conjugated polymers are hydrophobic and thus poorly dispersible in aqueous media, which limits polymer–water interfacial contact and hinders effective interaction with water and sacrificial agents (SAs) [80]. Furthermore, the formation of large polymer aggregates with low colloidal stability often occurs, reducing both dispersibility and light harvesting efficiency [87]. Despite these limitations, direct dispersion remains a valuable method for probing the intrinsic photophysical

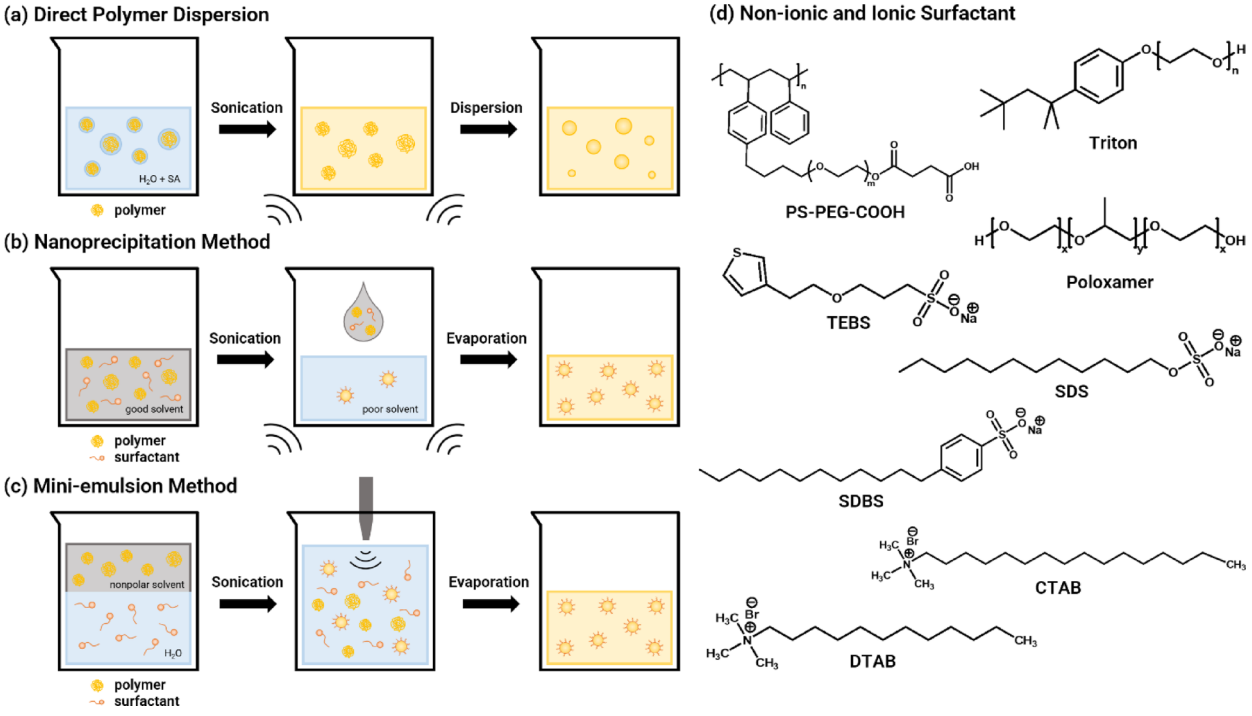


**Fig. 6** Fabrication methods for forming polymer-based photocatalyst nanoparticles: **a** direct polymer dispersion, **b** nanoprecipitation, **c** mini-emulsion method, and **d** non-ionic and ionic surfactants employed depending on the chosen method

properties of polymers in aqueous conditions, as it enables the study of polymer–solvent interactions and charge carrier dynamics without interference from surfactants or post-synthetic modifications [43, 67, 82].

For instance, Sachs et al. demonstrated that the extent of polymer–solvent interaction plays a critical role in governing colloidal behavior and photocatalytic activity in such systems. Linear conjugated polymers such as P1, P7, and P10 spontaneously assemble into micron- to submicron-sized aggregates in TEA/MeOH/$H_2O$ mixtures, yet are capable of generating long-lived photogenerated electrons even in the absence of surfactants or nanoparticle fabrication steps [43]. Although these dispersions exhibit relatively low surface area and weak light scattering compared to engineered nanoparticles, sulfone-containing polymers, most notably P10, achieved a HER of 3.3 mmol $g^{-1}$ $h^{-1}$ when dispersed in TEA/MeOH/$H_2O$ (1:1:1 v/v/v) under visible-light illumination. This result highlights that, even in minimally processed systems, the balance between polymer hydrophilicity, solvent affinity, and aggregation governs hole transfer to TEA and the subsequent yield of long-lived electron polarons, which ultimately determines photocatalytic performance.

### 3.2 Nanoparticle fabrication

To address the limitations of direct dispersion, nanoparticle fabrication has emerged as a central strategy in the development of polymeric photocatalysts. Techniques such as nanoprecipitation and mini-emulsion have been widely employed to produce well-dispersed polymer nanoparticles with controlled size, morphology, and colloidal stability (Fig. 6b, c; Table 1) [101, 102]. These methods increase the accessible interfacial area, enhance light harvesting, and facilitate charge transport, collectively contributing to improved photocatalytic efficiency [102]. Nanoparticle preparation traditionally relies on surfactants to stabilize dispersions and suppress aggregation; both ionic and non-ionic surfactants have been extensively used to generate stable and uniform nanoparticles [87, 102].

#### *3.2.1 Nanoprecipitation method*

In nanoprecipitation, a polymer is dissolved in a good solvent (e.g., THF), which sufficiently solvates the polymer chains and keeps them molecularly dispersed. This solution is then rapidly injected into a poor solvent (typically water), defined as a solvent in which the polymer has negligible solubility. The abrupt change in solvent quality induces polymer desolvation and chain collapse, leading to rapid aggregation and the formation of nanosized particles (Fig. 6b; Table 1) [103]. This simple method produces Pdots, typically stabilized by non-ionic surfactants such as PS–PEG–COOH, Triton, or Poloxamer [45, 104, 105]. The resulting nanoparticles exhibit enhanced dispersibility in aqueous media and improved charge transport due to their reduced size and increased surface area [102]. These features have been effectively demonstrated in several representative nanoprecipitation-based

**Table 1** Methods for direct polymer dispersion and the fabrication of polymer-based nanoparticles

| Method | Process description | Key parameters | Advantages | Limitations |
|---|---|---|---|---|
| Direct polymer dispersion | Polymer powders introduced into mixed solvents and tested directly for HER | Polymer-solvent affinity, solvent composition, and dispersion quality | Simple processing<br>Surfactant-free operation<br>Rapid activity screening<br>Intrinsic photophysics preserved | Aggregate formation<br>Low colloidal stability<br>High sensitivity to solvent composition<br>Hydrophilic polymer only |
| Nanoprecipitation | Rapid injection of a non-ionic surfactant-containing polymer solution into a poor solvent to form nanoscale particles | Solvent/non-solvent contrast, injection and mixing conditions, polymer concentration, and surfactant selection | Small, uniform nanoparticles<br>Improved aqueous dispersibility<br>Enhanced surface area and charge transport | Surfactant dependence<br>Solvent compatibility issues<br>Broad size distribution |
| Mini-emulsion | High-shear emulsification of a polymer in halogenated solvents with an ionic surfactant aqueous phase | Organic solvent selection, shear energy, surfactant type and concentration | Stable, well-dispersed nanoparticles<br>Morphology/structure tunability<br>Adaptable to various polymers | Surfactant dependence<br>Requirement for halogenated solvents<br>Scale-up challenges |

studies. Wang et al. employed PS–PEG–COOH as a stabilizer to encapsulate F8BT during nanoprecipitation, yielding uniform Pdots with diameters of approximately 30–50 nm [45]. These Pdots demonstrated improved water dispersibility, a red shift in absorption (~ 20 nm), and more efficient charge separation compared to bulk polymer powders. Under visible-light illumination (λ > 420 nm) in an aqueous solution containing 0.2 M ascorbic acid (AA) as an SA, these Pdots achieved HER of 8.3 mmol $g^{-1}$ $h^{-1}$, five orders of magnitude higher than that of pristine F8BT. Similarly, Elewa et al. reported a nanoprecipitation strategy to fabricate benzo[d][1,2,3] thiadiazole-based Pdots (PG4, PG6, PG7) by injecting THF-dissolved polymers into water containing Triton surfactant under sonication, followed by THF removal [104]. This method produced water-dispersible spherical nanoparticles (5–124 nm, depending on polymer type) with significantly reduced contact angles, from > 110° to 13–24°, enabling photocatalysis in the absence of organic co-solvents. Among these, PG6 Pdots exhibited stability exceeding 100 h, attributed to enhanced charge separation and halogen-induced electronic effects. These results demonstrate that nanoprecipitation is a simple and effective approach for rendering hydrophobic conjugated polymers operable under aqueous photocatalytic conditions.

#### *3.2.2 Mini-emulsion method*

In the mini-emulsion method, a polymer is first dissolved in an organic phase, typically using halogenated solvents such as chloroform to ensure good solubility, and then mixed with an aqueous phase containing surfactants, commonly anionic or cationic types such as sodium poly[2-(3-thienyl)ethoxy-4-butylsulfonate] (TEBS), sodium dodecyl sulfate (SDS), hexadecyl(trimethyl) ammonium bromide (CTAB), or dodecyltrimethylammonium bromide (DTAB), followed by high-shear homogenization or ultrasonication (Fig. 6c; Table 1) [106]. This method yields stable, size-controlled nanoparticles, with the surfactant identity exerting a significant influence on surface chemistry and internal morphology [102]. The implications of surfactant-dependent surface and morphological control are illustrated by the following studies. Dolan et al. reported single-component Y6 nanoparticles prepared via mini-emulsion, where Y6 was dissolved in chloroform and emulsified in an aqueous surfactant solution containing either TEBS or SDS, followed by ultrasonication and solvent evaporation [107]. Although both formulations exhibited similar optical absorption and transient photophysics, their photocatalytic activities differed substantially. Under sacrificial conditions with 2 wt% Pt and AA, TEBS-stabilized Y6 nanoparticles achieved an HER of 4.2 mmol $g^{-1}$ $h^{-1}$, while SDS-stabilized counterparts exhibited a 21-fold lower rate. TEM and zeta potential analyses revealed that SDS formed a dense, insulating layer that inhibited Pt photodeposition, whereas TEBS enabled efficient Pt loading and charge transfer. These findings indicate that the pronounced activity difference arises primarily from surfactant-controlled surface interactions rather than intrinsic photophysical disparities. Furthermore, Kosco et al. demonstrated that the mini-emulsion method offers precise control over D–A morphology in organic photocatalyst nanoparticles. PTB7-Th and EH-IDTBR were co-dissolved in chloroform and emulsified in an aqueous surfactant solution (SDS or TEBS), followed by ultrasonication and solvent evaporation to form stable dispersions [108]. The surfactant identity critically dictated the internal structure: SDS produced a core–shell morphology with a PTB7-Th-rich shell and EH-IDTBR core, which impeded both electron and hole extraction. In contrast, TEBS balanced interfacial energies to yield a more intermixed heterojunction, promoting efficient charge separation and Pt deposition. As a result, the HER increased nearly tenfold, reaching 64.0 mmol $g^{-1}$ $h^{-1}$, with an AQY

exceeding 6% at 700 nm. Collectively, these results demonstrate that mini-emulsion fabrication enables effective control over D–A interfaces, leading to enhanced hydrogen evolution performance.

#### *3.2.3 surfactant-free method*

While surfactant-assisted methods are generally effective for producing stable polymer nanoparticles, concerns persist that residual surfactants may block catalytic sites or alter interfacial properties [109]. To address this limitation, surfactant-free strategies have recently garnered increasing attention, as they yield cleaner particle surfaces by avoiding surfactant residues. However, these approaches typically require precise control over processing parameters to ensure long-term colloidal stability. The feasibility of this strategy is demonstrated by a recent study. Lin et al. developed surfactant-free bulk heterojunction polymer particles via miscibility-controlled co-precipitation of the relatively electron-rich polymer poly(5,10-bis(5-(2-butylocxyl)-2-thiophenyl)dithieno[2,3-d:2′,3′-d′]benzo[1,2-b:4,5-b′]dithiophene-*alt*-dibenzo[b, d]thiophene 5,5-dioxide) (PS) with the more electron-deficient polymer poly(5,10-bis(5-(2-butylocxyl)-2-thiophenyl)dithieno[2,3-d:2′,3′-d′]benzo[1,2-b:4,5-b′]dithiophene 1,1-dioxide-*alt*-dibenzo[b, d]thiophene 5,5-dioxide) (PSOS), both of which share nearly identical backbones [110]. This structural compatibility enables spontaneous and uniform D–A intermixing without the need for surfactants. The resulting particles exhibit clean interfaces, enhanced charge transfer, and reduced recombination, achieving an HER of 251.2 mmol $g^{-1}$ $h^{-1}$ and an AQY of 26.2% at 500 nm, significantly outperforming surfactant-stabilized analogues. Molecular simulations further reveal that surfactant layers can block electron-transfer sites and hinder proton accessibility, emphasizing that the surfactant-free design maximizes interfacial efficiency and catalytic activity. In a separate study, Bruder et al. prepared surfactant-free aqueous P3HT:$PC_{71}BM$ nanoparticles through nanoprecipitation from THF into water, employing $F_4TCNQ$ as a molecular dopant to induce electrostatic stabilization [111]. The dopant-mediated charge transfer between P3HT and $F_4TCNQ$ generated surface charges that effectively suppressed aggregation, yielding stable dispersions (~ 90–110 nm) with zeta potentials of approximately –43 mV and long-term stability exceeding ten weeks. These nanoparticles retained structural integrity during Pt photodeposition and sustained hydrogen evolution under visible-light illumination with AA as the SA. In contrast, the addition of SDS drastically reduced HER, confirming that surfactant layers impede charge transfer and limit catalytic performance. This study highlights that molecular-dopant-driven electrostatic stabilization enables the formation of surfactant-free polymer nanoparticles with cleaner interfaces and superior photocatalytic activity compared to their surfactant-containing counterparts.

## 4 Photophysical and structural insights into polymeric photocatalysts

Understanding how photocatalytic polymers absorb light, generate charge carriers, and organize structurally is essential for elucidating their photocatalytic behavior. These photophysical and structural characteristics not only define intrinsic material properties but also govern the mechanistic steps involved in photocatalytic hydrogen evolution [12]. Therefore, establishing clear correlations between structure, molecular properties, charge carrier dynamics, and catalytic function is fundamental to explaining hydrogen evolution at the molecular level. This section discusses the experimental techniques used to probe these properties, while the following section builds on these insights to describe the mechanistic pathways of photocatalytic proton reduction in polymer-based systems.

### 4.1 Experimental techniques for photophysical and structural analysis

#### *4.1.1 Optical absorption and emission-based techniques*

Optical spectroscopy forms the basis for evaluating how polymers interact with light (Fig. 7a; Table 2). UV–Vis absorption spectroscopy is widely used to assess the light-harvesting ability of polymeric photocatalysts, providing insights into absorption onset, spectral profile, and aggregation-induced spectral shifts [112]. For example, red- or blue-shifts in the absorption maximum (λmax), the emergence of shoulder bands, changes in bandwidth, or enhanced vibronic features can indicate increased aggregation, stronger π–π stacking, or variations in chain conformation and packing [70, 109]. However, such interpretations remain inferential and should ideally be corroborated by complementary structural characterization techniques.

Steady-state photoluminescence (PL) spectroscopy probes the radiative decay of excitons and is commonly used to investigate recombination pathways in polymeric photocatalysts [113]. Changes in PL intensity, peak position, or spectral shape can signal shifts in the balance between radiative and non-radiative recombination, alterations in exciton localization or migration, and modifications in aggregation state or inter-chain coupling within the polymer matrix [113–115]. Furthermore, PL quenching upon the addition of co-catalysts or SAs is frequently interpreted as evidence of charge transfer or exciton dissociation [116].

Tr-PL extends the insights offered by steady-state PL by measuring exciton lifetimes and distinguishing between radiative decay, non-radiative relaxation, and charge

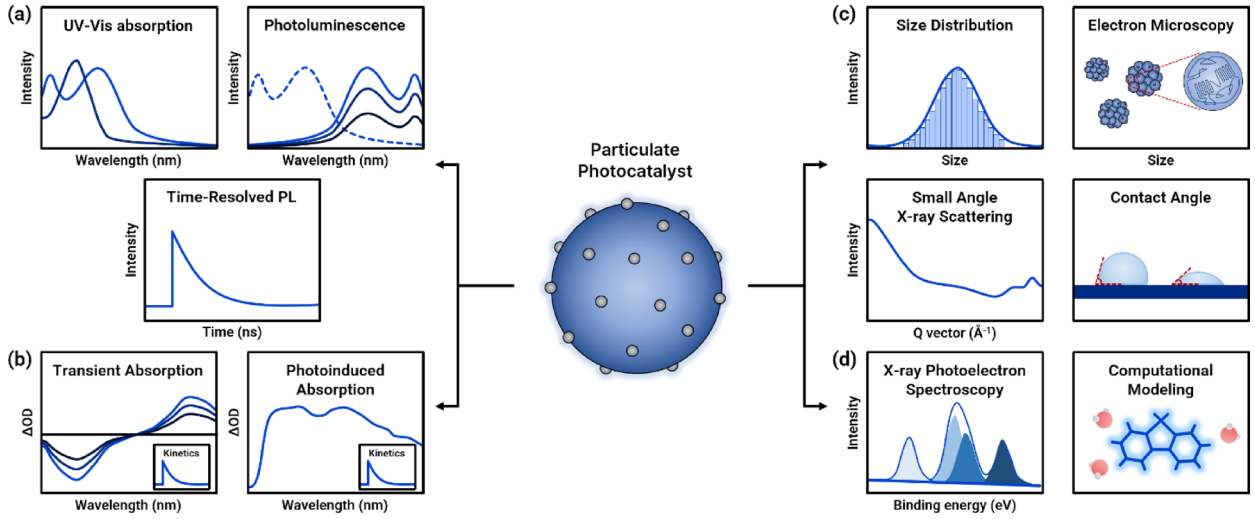


**Fig. 7** Techniques used for the characterization of photocatalytic particles: **a** optical techniques, **b** charge-carrier dynamics, **c** structural and morphological analysis, and **d** surface and interfacial characterization

transfer pathways [12]. Together, optical absorption and emission-based techniques elucidate the initial stages of the photocatalytic process, including photon absorption and exciton generation.

#### *4.1.2 Transient spectroscopy for charge carrier dynamics*

To investigate processes beyond exciton generation, transient spectroscopies are indispensable (Fig. 7b; Table 2). Femtosecond and nanosecond transient absorption spectroscopy (fs/ns-TAS) enable real-time observation of exciton decay, charge separation, polaron formation, and electron transfer to co-catalysts [102, 117]. In TAS spectra, two principal signals are typically analyzed: ground-state bleach (GSB) and photoinduced absorption (PIA). GSB appears as a negative signal at wavelengths corresponding to the ground-state UV–Vis spectrum, indicating depletion of ground-state populations upon photoexcitation [118]. In contrast, PIA manifests as positive absorption features associated with excited states or long-lived charge carriers such as polarons or triplet species [12, 118]. The temporal evolution of the GSB provides insight into exciton lifetime and recombination dynamics, while the decay or persistence of PIA signals reflects charge separation efficiency, carrier trapping, or interfacial electron transfer to co-catalysts [55, 119]. By combining femtosecond and nanosecond time windows, fs/ns-TAS captures the full sequence of photophysical events, from initial exciton formation to long-lived charge accumulation, thereby offering a powerful means to correlate transient charge dynamics with overall photocatalytic performance [55].

Photoinduced absorption spectroscopy (PIAS) complements TAS by probing long-lived photoexcited species, typically on microsecond to millisecond timescales [55]. Unlike TAS, which resolves ultrafast dynamics immediately following pulsed excitation, PIAS employs continuous or modulated illumination and monitors frequency-dependent changes in absorption, reflecting the quasi-steady-state accumulation of photogenerated charges [120, 121]. This technique enables identification of persistent polarons, trapped electrons, or charge-transfer states that dominate under near-operational photocatalytic conditions [55, 96]. Because the signal reflects the density and recombination dynamics of long-lived charge carriers rather than their instantaneous kinetics, PIAS offers direct insight into trap-limited recombination and dispersive transport processes, revealing whether photogenerated charges persist long enough to participate in catalytic hydrogen evolution [122, 123].

#### *4.1.3 Structural and morphological characterization*

The structural arrangement of polymer particles plays a critical role in governing light harvesting, charge transport, and polymer–water interactions (Fig. 7c; Table 2) [43, 102]. Dynamic light scattering (DLS) is widely employed to assess the hydrodynamic size and size distribution of polymeric photocatalyst particles dispersed in liquid media [102]. In addition to particle size analysis, DLS is often complemented by zeta potential measurements, which quantify the electrostatic potential at the particle–solvent interface [107]. Zeta potential serves as a key indicator of colloidal stability, with large absolute values (typically $|\zeta| > 30$ mV) suggesting sufficient interparticle repulsion to prevent aggregation [124, 125]. The combined information on particle size and surface charge makes DLS a practical and informative technique for evaluating the formation and stability of polymer dispersions or nanoparticles in photocatalytic systems.

**Table 2** Experimental techniques commonly employed in the characterization and performance evaluation of photocatalytic polymers

| Techniques | Measured quantity/Probe | Key information | Relevance to photocatalysis |
|---|---|---|---|
| UV-Vis absorption | Absorption spectrum/onset, λmax, vibronic structure, spectral shift | Light-harvesting ability & optical bandgap<br>Aggregation/π-π stacking strength<br>Chain conformation | Photon absorption profile<br>Aggregation effects on exciton generation |
| PL | Emission intensity, peak position, spectral shape, quenching yield | Radiative/non-radiative recombination<br>Exciton localization/migration<br>Aggregation state<br>Charge transfer (via quenching) | Recombination pathways<br>Exciton quenching & charge separation |
| Tr-PL | Exciton lifetime decay, decay components | Radiative/non-radiative rates<br>Charge-transfer signatures<br>Excited-state dynamics | Exciton dissociation kinetics<br>Lifetime to charge separation efficiency |
| TAS | Ground-state bleach (GSB), photo-induced absorption (PIA), transient spectra, excited-state kinetics | Exciton decay<br>Charge separation<br>Polaron/triplet formation<br>Electron transfer | Exciton dissociation/recombination<br>Charge transfer dynamics<br>Transient carrier lifetime to HER |
| PIAS | Modulated photo-induced absorption, long-lived carrier signals | Persistent polarons/trapped electrons<br>Long-lived recombination<br>Steady-state charge accumulation | Whether charges survive to drive HER<br>Trap-limited transport<br>Operational charge density |
| DLS | Hydrodynamic diameter, size distribution, zeta potential (surface electrostatic potential) | Particle size & dispersity<br>Colloidal stability<br>Aggregation degree | Dispersion quality<br>Polymer-solvent interaction and aggregation effects on charge transport |
| TEM | Internal morphology, porosity, phase-separated domains, metal distribution (HR-TEM, EDS), native-state morphology (cryo-TEM) | Nanostructure<br>Polymer-metal interface<br>True dispersion state | Internal morphology governing charge carrier transport and separation efficiency<br>Co-catalyst nanoparticle size, dipersion, and anchoring<br>Hydrated-state morphology |
| SEM | Surface morphology, particle shape, size uniformity | Surface texture<br>Aggregation state<br>Dry-state geometry | Particle aggregation<br>Surface roughness/porosity<br>Co-catalyst deposition behavior |
| SAXS | Small-angle scattering profiles | Aggregate size/shape<br>Internal density<br>Nanoscale morphology | Correlation of nanoscale organization with charge transport & catalytic efficiency |
| Contact angle | Static wetting angle | Surface hydrophilicity/hydrophobicity<br>Surface functionalization effects | Polymer-water compatibility and proton accessibility during HER |
| XPS | Elemental composition, oxidation states, binding-energy shifts, surface chemical environment | Heteroatom incorporation<br>Co-catalyst deposition and oxidation state<br>Surface chemistry | Surface states & charge transfer governing proton reduction |
| MD | Hydration structure, solvent penetration, interface stability | Polymer-water interactions<br>Hydrophilic/hydrophobic domains | Interfacial environment affecting charge extraction and HER |
| DFT | Electrostatic potential, orbital energies, charge localization, proton-binding sites | Band alignment<br>Reaction sites<br>Electronic structure | Molecular design-proton reduction energetics relationship |

Transmission and scanning electron microscopy (TEM and SEM) enable visualization of particle morphology, internal porosity, and co-catalyst deposition [96, 126]. SEM provides surface-level information such as particle shape, size uniformity, and surface texture, while TEM offers higher-resolution imaging capable of revealing internal nanostructures, including porosity and phase-separated domains [102, 127, 128]. In systems incorporating metal co-catalysts (e.g., Pt, Pd), TEM can also be used to observe metal deposition, spatial distribution, and polymer–metal interfaces [96]. These observations are often complemented by high-resolution TEM (HR-TEM) or energy-dispersive X-ray spectroscopy (EDS) for lattice imaging and elemental mapping, respectively [129, 130]. Because polymeric photocatalysts are typically dispersed in aqueous or mixed-solvent environments, conventional dry-state TEM may not accurately reflect their native morphology. To overcome this limitation, cryo-TEM, where samples are rapidly vitrified to preserve their liquid-phase structure, or liquid-phase TEM techniques are increasingly utilized to image polymer nanoparticles and colloidal dispersions under near-operational conditions [119, 131].

Small-angle X-ray scattering (SAXS) is a powerful technique for probing nanoscale structural features in polymeric photocatalysts [132]. Unlike diffraction-based

methods that assess long-range crystalline order, SAXS provides information on particle size, shape, internal density fluctuations, and spatial organization of polymer aggregates in solution [132]. As an ensemble-averaged method, SAXS serves as a valuable complement to imaging and diffraction techniques, offering statistically robust insights into polymer morphology.

Water contact angle measurements are also commonly used to assess the surface wettability of polymeric photocatalysts by determining the angle formed between a liquid droplet and the solid surface [133]. A smaller contact angle indicates higher surface hydrophilicity, while a larger angle signifies hydrophobicity [133]. This technique is particularly useful for evaluating surface modifications, such as side-chain functionalization or heteroatom incorporation that influence polymer–water interactions [127, 134]. Although it does not provide molecular-level structural information, contact angle analysis offers a simple and quantitative means to compare surface properties across different polymer materials. Collectively, these characterization techniques not only reveal particle architecture and interfacial properties but also contribute to a mechanistic understanding of how structural features influence overall photocatalytic activity.

#### *4.1.4 Surface and interface characterization*

Since photocatalytic reactions occur at the catalyst–solution interface, surface-sensitive techniques are essential (Fig. 7d; Table 2). X-ray photoelectron spectroscopy (XPS), which probes the top few nanometers of polymer photocatalysts, provides detailed information on elemental composition, oxidation states, and local electronic environments [135]. It is particularly effective for confirming the incorporation of heteroatoms, monitoring co-catalyst deposition, and detecting interfacial charge transfer via binding-energy shifts [74, 136, 137]. By correlating these surface chemical changes with photocatalytic activity, XPS offers critical insights into how surface chemistry governs proton reduction and overall hydrogen evolution.

Molecular dynamics (MD) simulations complement these findings by offering atomistic insight into polymer–water interactions, including hydration structure, solvent penetration, and interfacial stability [43, 66, 82]. They enable quantitative analysis of how hydrophilic and hydrophobic domains influence water diffusivity and the extent of polymer–water contact, providing molecular-level understanding in systems where experimental observation of interfacial dynamics is limited.

Density functional theory (DFT) calculations further elucidate electrostatic potential (ESP) distributions, charge localization, band alignment, and potential proton adsorption sites [82, 86, 138]. Through electronic structure analysis, DFT enables prediction of how molecular design, such as heteroatom incorporation or side-chain modification, affects frontier orbital energies and facilitates proton reduction [12, 139]. These calculations also offer insight into the strength and geometry of proton-binding interactions on polymer backbones or co-catalyst interfaces, establishing a theoretical framework for interpreting experimental trends in photocatalytic activity.

Together, these experimental and theoretical approaches reveal how interfacial properties dictate charge extraction and catalytic performance, thereby linking molecular-level interactions to overall hydrogen evolution efficiency.

A comprehensive understanding of polymeric photocatalysts requires establishing clear connections between their photophysical behavior and structural features. As summarized above, optical and transient spectroscopies elucidate how excitons are generated, migrate, and decay, while morphological, surface, and computational analyses clarify how particle structure, interfacial characteristics, and electronic configuration influence these processes. Together, these insights define key structure–property relationships that govern hydrogen evolution.

To move beyond phenomenological observation and achieve a deeper understanding of photocatalysis, it is essential to link these properties to the individual reaction steps. In the following section, we therefore examine the mechanistic pathways of photocatalytic hydrogen evolution, from light absorption and charge transport to interfacial proton reduction.

### 4.2 Mechanistic pathways of photocatalytic hydrogen evolution

#### *4.2.1 Photon absorption and exciton generation*

When a polymer absorbs photons, excitons are generated due to the low dielectric constant of organic materials (Fig. 8a) [140]. The efficiency of photocatalysis depends strongly on how effectively these excitons are dissociated into free charges [141]. Accordingly, various strategies have been developed to enhance light absorption and charge separation efficiency. For example, Elsayed et al. investigated ITIC-based polymers incorporating different π-linkers to examine how linker-induced variations in conjugation length and backbone planarity influence light absorption and exciton dynamics [109]. The introduction of difluorothiophene (ThF) linkers broadened absorption into the near-infrared (NIR) region and reduced the optical bandgap from 2.05 eV to 1.55 eV by enhancing π–π stacking interactions. fs-TAS revealed slower bleach recovery and prolonged charge-separated states, indicating more efficient charge delocalization between acceptor units and suppressed recombination. Theoretical calculations confirmed that the ThF linker

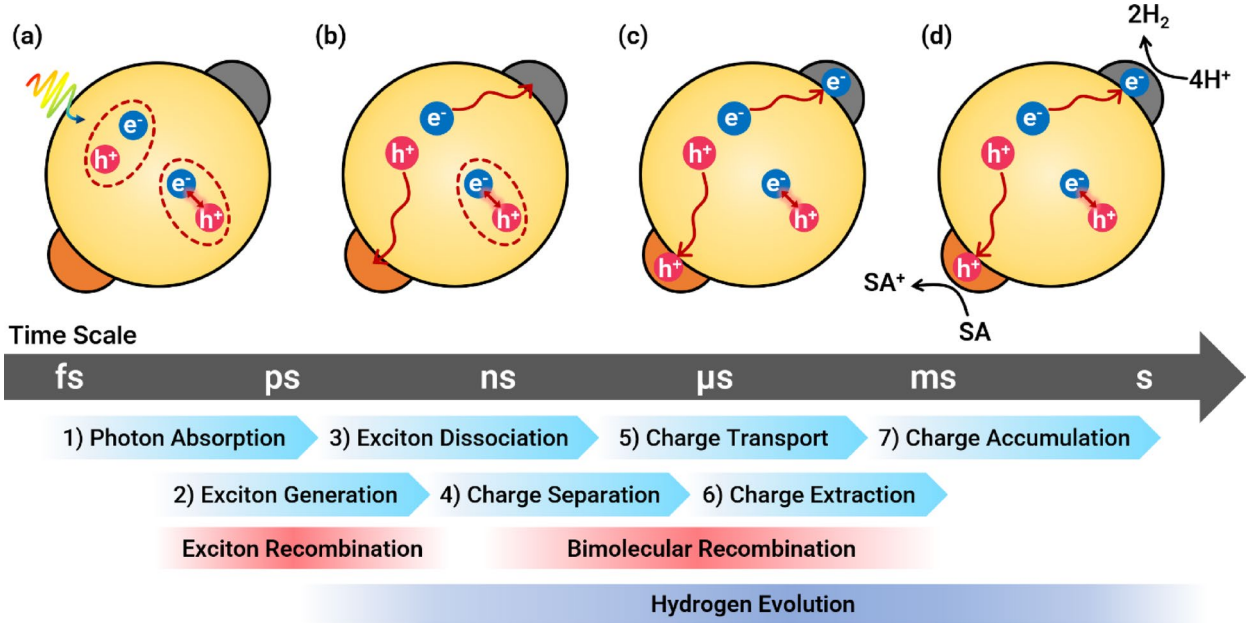


**Fig. 8** Reaction behavior of polymer photocatalysts for hydrogen evolution across characteristic time scales: **a** photon absorption and exciton generation, **b** exciton dissociation and charge separation, **c** charge transport and extraction, and **d** charge accumulation and hydrogen evolution

reduces the dihedral angle and strengthens electronic coupling between adjacent acceptors, thereby facilitating more effective charge separation. As a result, PITIC-ThF nanoparticles exhibited a HER of 339.7 mmol $g^{-1}$ $h^{-1}$ under visible-light illumination and 4.1 mmol $g^{-1}$ $h^{-1}$ under NIR illumination, highlighting π-linker engineering as a powerful strategy to improve both photon absorption and charge utilization.

#### *4.2.2 Exciton dissociation and charge separation*

Exciton dissociation typically occurs at sites where sufficient energetic driving forces or favorable interfacial environments allow excitons to separate into free charges (Fig. 8b) [142]. This process is strongly influenced by molecular design, interfacial engineering, and the surrounding medium, all of which determine how efficiently charges are generated for subsequent photocatalytic reactions [143, 144]. In contrast, excitons that fail to dissociate undergo radiative or non-radiative recombination, releasing energy as light or heat rather than contributing to charge generation, thereby reducing overall photocatalytic efficiency [145]. To address this limitation, Kosco et al. demonstrated that introducing oligo(ethylene glycol) (OEG) side chains into conjugated polymers significantly enhances intrinsic charge generation and separation in both neat and D–A nanoparticles [144]. Glycolation increased the dielectric constant and water uptake, facilitating ultrafast exciton-to-polaron conversion (~ 8 ps) and suppressing both geminate and non-geminate recombination. In gIDTBT:oIDTBR nanoparticles, the resulting higher yield of long-lived polarons enabled efficient hole scavenging by AA, achieving a HER of 18.5 mmol $g^{-1}$ $h^{-1}$, 30-fold higher than that of the non-glycolated analogue. The enhanced dielectric environment and hydrophilicity induced by glycolation effectively reduced electrostatic binding within excitons and charge-transfer states, stabilized charge carriers, and demonstrated side-chain dielectric engineering as a powerful strategy for boosting photocatalytic hydrogen evolution.

#### *4.2.3 Charge transport and recombination*

Once separated, charge carriers migrate through the polymer matrix toward interfaces where catalytic reactions occur (Fig. 8c) [12]. Their mobility and lifetime are strongly influenced by the material's overall structural organization and local environment [146]. While well-ordered domains and continuous pathways promote efficient charge transport, disordered regions or energetic traps can redirect carriers into recombination processes [97, 98]. Such recombination, whether from free charges or bound excitons, acts as a major loss channel that ultimately limits photocatalytic efficiency [12]. To mitigate recombination losses, strategies such as enhancing crystallinity or achieving optimized phase segregation have been explored. An et al. demonstrated that fluorination of BT-based conjugated polymers induces strong intrachain $S^{\delta+}$–$F^{\delta-}$ interactions, which enhance backbone planarity and promote tighter π–π stacking (3.55 Å), thereby facilitating efficient charge transport [147]. Compared to the OEG-only analogue, the fluorinated polymer (P3) exhibited significantly improved crystallinity and dielectric properties, leading to suppressed

geminate recombination. TAS revealed that P3 generated long-lived charge carriers persisting up to 14 μs, in contrast to the rapid nanosecond-scale decay observed in the non-fluorinated analogue, confirming reduced charge recombination and more effective charge transfer to protons. As a result, P3 achieved a HER of 26.0 mmol $g^{-1}$ $h^{-1}$ under visible light illumination (> 420 nm). This correlation between fluorination-induced structural ordering and TAS-observed carrier lifetimes underscores the critical role of backbone planarity in enabling efficient charge transport for photocatalytic hydrogen evolution.

#### *4.2.4 Charge extraction and accumulation at the interface*

After migrating through the polymer matrix, photogenerated charge carriers must be extracted at the polymer–solution interface to initiate redox reactions (Fig. 8d). Electrons are transferred from the polymer to co-catalyst sites, typically Pt, Pd, or Ir, where they drive proton reduction [73, 74, 137]. Simultaneously, photogenerated holes are consumed by SAs, such as amines, alcohols, or organic acids, to prevent charge accumulation and suppress recombination [70, 73, 77]. The efficiency of interfacial charge extraction is governed by (i) the energetic alignment between the polymer's frontier orbitals and the redox potentials of the co-catalyst and sacrificial species, (ii) the interfacial energetics and proton adsorption–desorption kinetics, which determine how efficiently protons are reduced or released at the interface, and (iii) the stability of the dispersion medium, which affects whether charge carriers can effectively reach catalytic sites [43, 137, 148, 149]. Optimizing these parameters enhances charge extraction, thereby directly coupling photophysical charge generation with catalytic function. To exemplify this mechanism, Bai et al. demonstrated that the linear conjugated polymer P10, co-loaded with Pd and Ir, can perform overall water splitting under visible light for over 60 h [137]. Although Ir was initially deposited as metallic Ir nanoparticles, operando and XPS analyses confirmed its rapid in situ oxidation to $IrO_2$ under water oxidation conditions, identifying $IrO_2$ as the active OER co-catalyst. At the polymer–solution interface, electrons were transferred to Pd for proton reduction, while holes were efficiently extracted by $IrO_2$ to drive water oxidation. TAS revealed ultrafast hole transfer (< 2 ps) from P10 to $IrO_2$, forming a long-lived $P10^{(-)}/IrO_2^{(+)}$ charge-separated state that effectively suppressed recombination. These findings illustrate how co-catalyst engineering enhances interfacial charge separation and couples photophysical charge generation with catalytic water splitting via improved polaron formation. In a separate study, Liang et al. introduced a σ–π anchoring strategy to improve charge extraction at the polymer–solution interface [149]. The Y6CO molecule, a Y6 derivative containing a core carbonyl group, forms strong σ–π coordination with Pt, stabilizing metallic $Pt^0$ and accelerating the in situ photoreduction of $Pt^{II}$ to $Pt^0$. XPS revealed a higher $Pt^0$ ratio in Y6CO/Pt (84.2%) compared to Y6/Pt (63.6%), while FT-IR redshifts indicated enhanced π-backdonation. This coordination doubled the $Pt^{II} \rightarrow Pt^0$ reduction rate and lowered the $H^*$ adsorption energy to −0.077 eV, facilitating $H_2$ evolution. As a result, Y6CO nanoparticles achieved a HER of 231.0 mmol $g^{-1}$ $h^{-1}$, while PM6:Y6CO heterojunctions reached 323.2 mmol $g^{-1}$ $h^{-1}$ with an AQY of 11.6% at 700 nm. These results demonstrate how anchoring strategies enhance charge extraction and suppress recombination, thereby outperforming non-anchored systems.

#### *4.2.5 Hydrogen evolution reaction*

Once electrons are successfully delivered to co-catalyst sites, the hydrogen evolution reaction proceeds via proton reduction (Fig. 8d). As discussed in Sect. 4.2.4, the kinetics and efficiency of the hydrogen evolution reaction depend heavily on the catalytic properties of the co-catalyst. Noble metals such as Pt, Pd, and Ir exhibit nearly ideal hydrogen adsorption–desorption energetics, enabling rapid turnover frequencies and low overpotentials [150]. To address issues of cost and sustainability, alternative materials such as transition metal carbides, sulfides, and phosphides have been investigated; however, their catalytic activities vary considerably with composition, surface states, and morphology [151–153]. In parallel, co-catalyst-free strategies, wherein the polymer itself provides active sites for proton reduction, have emerged as viable approaches, offering the potential to reduce material costs and simplify catalyst architecture [109–111].

On the oxidative side, SAs play a critical role in stabilizing the overall photocatalytic process by consuming photogenerated holes. The choice of SA affects not only the reaction pathway but also the long-term stability of the system [154, 155]. Inefficient hole scavenging can lead to charge accumulation, increased recombination rates, and photocorrosion, emphasizing the need to balance both the reduction and oxidation half-reactions [139]. Although the role of SAs is often reduced to their electron-donating capacity, their chemical environment, particularly the pH, significantly influences photocatalytic performance. While it is commonly assumed that acidic conditions enhance hydrogen evolution by providing a high concentration of protons, widely used SAs such as trimethylamine (TEA) and triethanolamine (TEOA) generate alkaline conditions yet still enable efficient hydrogen production [70, 86, 156, 157]. This observation suggests that overall photocatalytic efficiency is not governed solely by the bulk pH of the solution. Instead, multiple factors contribute, including the protonation state and oxidation potential of the SA, the nature and

reactivity of intermediate radicals, and the local pH environment at the polymer–water interface [43, 66, 82]. Therefore, a comprehensive understanding of the interplay between SA chemistry and photocatalytic pathways is essential for the rational design of more efficient hydrogen evolution systems.

Overall, the seamless integration of charge generation, transport, interfacial charge extraction, and catalytic proton reduction is essential for achieving optimal hydrogen evolution performance. Only when these processes are effectively harmonized can polymeric photocatalysts realize their full potential, highlighting the importance of coordinated molecular design, interface engineering, and catalytic optimization for practical solar-to-hydrogen conversion.

## 5 Evaluation methodologies of HER

Reliable evaluation methodologies are critical for assessing the performance of polymeric photocatalysts, typically by quantifying the evolved hydrogen using gas chromatography (GC), and for enabling meaningful comparisons across different systems (Fig. 9a) [158]. The quantitative data obtained from GC measurements form the basis for calculating key performance metrics, including the HER, AQY, and solar-to-hydrogen (STH) efficiency. Despite significant progress, the field lacks universally accepted protocols for evaluating and comparing the performance of organic photocatalysts, which continues to hinder direct cross-study comparisons and reproducibility. This section discusses the primary efficiency metrics used to quantify photocatalytic performance and examines current challenges in establishing standardized evaluation practices.

### 5.1 Efficiency metrics

#### *5.1.1 HER*

The HER remains the most frequently reported parameter for evaluating photocatalytic systems. It is typically expressed in μmol $g^{-1}$ $h^{-1}$ or mmol $g^{-1}$ $h^{-1}$, representing the mass-specific rate of hydrogen generation under illumination (Fig. 9b) [66, 109, 147]. Although mass-normalized HER is the standard reporting format, various alternative units are employed depending on reactor configuration and measurement objectives. For example, when catalysts are immobilized as thin films or coatings, HER is often reported per illuminated area (mmol $h^{-1}$ $cm^{-2}$ or mmol $h^{-1}$ $m^{-2}$) rather than per unit mass [96, 159]. In systems where the catalyst mass cannot be accurately determined, HER may be expressed as a total, unnormalized value (mmol $h^{-1}$) [85, 86, 137]. Volume-based units (mmol $L^{-1}$) are also used when comparing reactions under identical solution conditions [160].

While these unit variations offer system-specific insights, they also complicate quantitative comparisons across studies, underscoring the need for unified reporting protocols. HER remains valuable for benchmarking relative performance trends within a single study, for instance, when comparing polymers with different molecular structures, particle sizes, or co-catalyst loadings. However, because HER is highly sensitive to

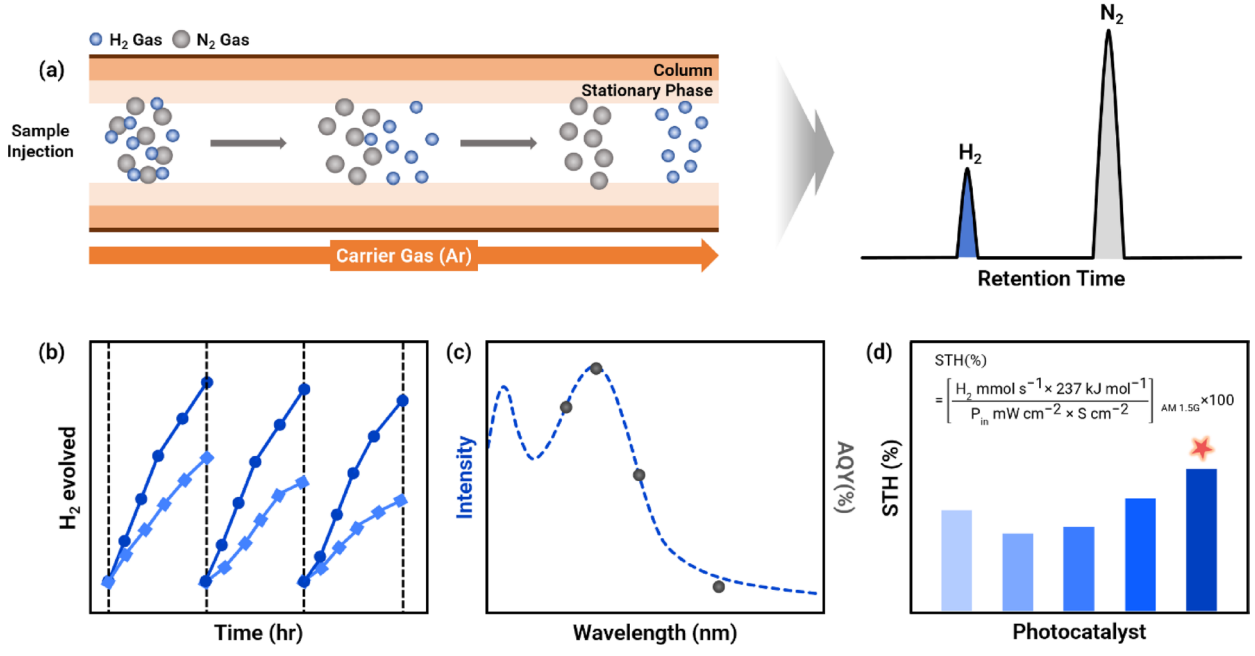


**Fig. 9** Methodologies and representations used for evaluating hydrogen-production performance: **a** gas chromatography–based separation of gaseous products and appearance of corresponding peaks in the chromatogram, **b** graphical representation of hydrogen-evolution performance, **c** depiction of apparent quantum yield (AQY) and **d** calculation and expression of solar-to-hydrogen (STH) conversion efficiency

experimental parameters such as light intensity, spectral distribution, SA type, co-catalyst content, and reactor geometry, it is not inherently suitable for cross-study comparisons unless experimental conditions are standardized [161].

#### *5.1.2 AQY*

The AQY provides a wavelength-specific measure of photocatalytic efficiency, defined as the ratio of hydrogen molecules evolved to the number of incident photons at a given wavelength (Fig. 9c) [162]. AQY directly links optical absorption to catalytic output, offering mechanistic insight into how effectively absorbed photons are converted into chemical products [96]. It is commonly calculated as: AQY (%) = (2 × number of $H_2$ molecules evolved / number of incident photons) × 100 [70]. The factor of two accounts for the two electrons required to generate one $H_2$ molecule. Notably, this expression does not include a term for catalyst mass. Consequently, increasing the photocatalyst loading can artificially inflate AQY values, highlighting the need for complementary metrics that normalize activity with respect to catalyst mass.

Despite these limitations, AQY remains a critical parameter for benchmarking photocatalytic performance across different excitation wavelengths [96, 108]. In practical hydrogen-evolution systems, AQY should be reported alongside HER and catalyst loading conditions to enable comprehensive assessment, not only of how many photons are converted, but also how many hydrogen molecules are produced per unit mass of photocatalyst under comparable illumination conditions.

#### *5.1.3 STH*

The most rigorous and practically relevant metric for photocatalytic water splitting is the STH efficiency, which quantifies the overall conversion of incident solar energy into chemical energy stored in hydrogen (Fig. 9d) [163]. It is calculated by dividing the chemical energy of the evolved $H_2$, obtained by multiplying the rate of hydrogen production with the standard Gibbs free energy required to produce one mole of $H_2$ from water ($\Delta G^\circ \approx 237$ kJ $mol^{-1}$), by the total incident solar power under AM 1.5G illumination (Fig. 9d) [163]. Unlike HER and AQY, STH must be determined under unbiased conditions without the use of SAs, making it a stringent benchmark for evaluating photocatalyst performance in real-world applications [164]. While STH is routinely reported for inorganic photocatalysts, it remains rarely demonstrated in polymeric systems due to the inherent challenges of achieving overall water splitting and maintaining long-term stability under true solar conditions [165, 166]. These and other related challenges will be discussed in the next section.

### 5.2 Challenges in standardization

Despite advancements in reporting photocatalytic performance, several challenges persist in establishing standardized evaluation protocols for polymeric systems. A major issue is the absence of unified reporting formats, as studies often present HER, AQY, or STH efficiency using inconsistent units, experimental setups, and illumination sources (Table 3). In particular, HER is variously normalized to catalyst mass, reaction volume, or illuminated area, hindering direct comparison across publications [109, 159, 160]. Cross-laboratory reproducibility further complicates this issue. Variations in light intensity calibration, reactor design, and gas analysis methods can lead to significant discrepancies in reported values [66, 77, 86]. Even minor differences in SA concentration or co-catalyst deposition can substantially influence the observed rates, highlighting the sensitivity of polymeric systems to experimental conditions [74, 136, 137]. To address these challenges, several standardization recommendations can be proposed. These include reporting HER in consistent units with complete experimental details; measuring and reporting AQY using calibrated monochromatic light sources with accurately determined photon flux; and, whenever possible, presenting unbiased STH values under AM 1.5G illumination for fair benchmarking [161–164, 167, 168]. Additionally, the adoption of internal standards and inter-laboratory round-robin tests could enhance reproducibility and improve the reliability of reported results.

## 6 Future perspectives

Future progress in polymeric photocatalysts will require a more integrated approach that unifies molecular design, particle engineering, and photophysical analysis. While each strategy has independently led to notable advancements, their combined application holds the greatest promise for comprehensive optimization. Molecular engineering enables the tuning of fundamental polymer properties; particle-level design enhances processability and catalytic accessibility; and photophysical studies elucidate structure–performance relationships. Together, these dimensions can support the development of rational design rules for next-generation polymeric photocatalysts. Building on this integrated perspective, future efforts should focus on translating molecular- and particle-level design concepts into actionable and testable design frameworks.

Emerging technologies further offer opportunities to accelerate discovery. Such framework-oriented approaches, which often involve highly multidimensional and interdependent design variables, naturally motivate the adoption of data-driven and high-throughput methodologies capable of navigating complex design spaces.

**Table 3** Reported polymeric photocatalysts and their hydrogen evolution performances under various experimental conditions

| Photocatalyst | Fabrication method | Stabilizer | Amount of catalyst | Reactor | Light source | Reaction medium | Co-catalyst | HER | AQY | References |
|---|---|---|---|---|---|---|---|---|---|---|
| P10 | Direct polymer dispersion | - | 25 mg | Flask | 300 W Xenon lamp (λ > 420 nm) | 22.5 mL of TEA: MeOH: $H_2O$ (1:1:1 v/v/v) | 0.4 wt% residual Pd | 3.3 mmol $g^{-1}$ $h^{-1}$ | 11.6 ± 0.5@420 nm | [43] |
| P-2$SO_2$ | Direct polymer dispersion | - | 2 mg | Reaction glass container | 350 W Xenon lamp (λ = 380–780 nm, 1000 W $m^{-2}$) | 10 mL of 1 M AA in NMP: $H_2O$ (1:9 v/v, pH 4) | 3 wt% $H_2PtCl_6$ | 0.4 mmol $h^{-1}$ | 37.5@420 nm | [60] |
| FS5 | Direct polymer dispersion | - | 25 mg | Quartz flask | 300 W Xenon lamp (AM 1.5G, λ > 420 nm, 1000 W $m^{-2}$) | 22.5 mL of TEA: MeOH: $H_2O$ (1:1:1 v/v/v) | - | 1.4 mmol $g^{-1}$ $h^{-1}$ | 2.1@420 nm | [66] |
| P7 | Direct polymer dispersion | - | 25 mg | Flask | 300 W Xenon lamp (λ > 295 nm) | 22.5 mL of trimethylamine (TEA): methanol (MeOH): $H_2O$ (1:1:1 v/v/v) | - | 0.2 mmol $h^{-1}$ | 2.3@420 nm | [70] |
| P-FSO | Direct polymer dispersion | - | 50 mg | Pyrex top-irradiation reaction vessel | 300 W Xenon lamp (λ > 420 nm) | 110 mL of triethanolamine (TEOA): $H_2O$ (1:10 v/v/v) | 1.07 wt% residual Pd | 0.4 mmol $h^{-1}$ | 8.5@420 nm | [73] |
| PAE-D | Direct polymer dispersion | - | 50 mg | Pyrex top-irradiation reaction vessel | 300 W Xenon lamp (λ > 300 nm) | 110 mL of TEOA: $H_2O$ (1:10 v/v) | 3 wt% Pt | 0.2 mmol $h^{-1}$ | 5.6@420nm | [74] |
| PBDTTS–1SO | Direct polymer dispersion | - | 2 mg | Reaction glass | 350 W Xenon lamp (AM 1.5G, λ = 380–780 nm, 1000 W $m^{-2}$) | 10 mL of 1 M ascorbic acid (AA) in N-methyl-2-pyrrolidone (NMP): $H_2O$ (1:9 v/v, pH 4) | 3 wt% $H_2PtCl_6$ | 97.1 mmol $g^{-1}$ $h^{-1}$ | 18.5@500 nm | [77] |
| P8-i | Direct polymer dispersion | - | 25 mg | Quartz flask | 300 W Xenon lamp (λ > 295 nm) | 22.5 mL of TEA: MeOH: $H_2O$ (1:1:1 v/v/v) | - | 0.9 mmol $g^{-1}$ $h^{-1}$ | - | [80] |

**Table 3** (continued)

| Photocatalyst | Fabrication method | Stabilizer | Amount of catalyst | Reactor | Light source | Reaction medium | Co-catalyst | HER | AQY | References |
|---|---|---|---|---|---|---|---|---|---|---|
| FS-TEG | Direct polymer dispersion | - | 25 mg | Quartz flask | 300 W Xenon lamp (λ > 420 nm) | 25 mL of TEA: MeOH: $H_2O$ (1:1:1 v/v/v) | - | 2.9 mmol $g^{-1}$ $h^{-1}$ | 10.0@420 nm | [82] |
| COP-PB-N2 | Direct polymer dispersion | - | 5 mg | 60 ml quartz tube | 300 W Xenon lamp (λ > 400 nm) | 24 mL of TEA: MeOH: $H_2O$ (1:1:10 v/v/v) | - | 0.05 mmol $h^{-1}$ | 35.5@400 nm | [84] |
| TPT-TPT-CMP | Direct polymer dispersion | - | 10 mg | 35 mL Pyrex reactor | 350 W Xenon light (λ = 380–780 nm, 1000 W $m^{-2}$) | 20 mL of TEA: MeOH: $H_2O$ (1:1:1 v/v/v) | - | 0.1 mmol $h^{-1}$ | 32.4@420 nm | [85] |
| B-FOBT–1,4-E | Direct polymer dispersion | - | 30 mg | Pyrex top irradiation reaction vessel | 300 W Xenon lamp (λ > 420 nm) | 30 mL of TEOA/$H_2O$ (1:9 v/v) | 0.3 wt% residual Pd | 0.4 mmol $h^{-1}$ | 5.7@420 nm | [86] |
| S-CMP3 | Direct polymer dispersion | - | 25 mg | Flask | 300 W Xenon lamp (λ > 420 nm) | 25 mL of TEA: MeOH: $H_2O$ (1:1:1 v/v/v) | - | 3.1 mmol $g^{-1}$ $h^{-1}$ | 13.2@420 nm | [90] |
| TATR-PPN | Direct polymer dispersion | - | 5 mg | Vial | 150 W Xenon lamp (λ > 420 nm, 1000 W $m^{-2}$) | 10 mL of 1 M AA in DMF: $H_2O$ (2:8 v/v) | 1 wt% $H_2PtCl_6$ | 7.2 mmol $g^{-1}$ $h^{-1}$ | 6.6@420 nm | [136] |
| P10/Ir | Direct polymer dispersion | - | 1 mg | Top-irradiation cell | 300 W Xenon lamp (AM 1.5G, λ > 420 nm, 1000 W $m^{-2}$) | 120 mL of $H_2O$ | 1 wt% $NH_4IrCl_6$ | 0.006 mmol $h^{-1}$ (OER: 0.002 mmol $h^{-1}$) | 0.1@350 nm | [137] |
| PS-OTEG | Direct polymer dispersion | - | 25 mg | 64 mL quartz flask | 300 W Xenon lamp (λ > 420 nm) | 22.5 mL of TEA: MeOH: $H_2O$ (1:1:1 v/v/v) | 0.52 wt% residual Pd | 1.8 mmol $g^{-1}$ $h^{-1}$ | 5.3@420 nm | [139] |
| P3 | Co-solvent method | Methanol | 1 mg | 50 mL quartz flask | 300 W Xenon lamp (λ > 420 nm) | 0.2 M AA in MeOH: water (4:6 v/v) | - | 26.0 mmol $g^{-1}$ $h^{-1}$ | 2.2@600 nm | [147] |

**Table 3** (continued)

| Photocatalyst | Fabrication method | Stabilizer | Amount of catalyst | Reactor | Light source | Reaction medium | Co-catalyst | HER | AQY | References |
|---|---|---|---|---|---|---|---|---|---|---|
| 4CzIPN | Direct polymer dispersion | - | 5 mg | Two-neck quartz reactor | 300 W Xenon lamp (λ > 400 nm) | 16 mL of TEOA: $H_2O$ (1:4 v/v, pH 10.7) | 8 wt% $H_2PtCl_6$ | 0.7 mmol $h^{-1}$ $m^{-2}$ | 0.3@365 nm | [159] |
| LS2 | Direct polymer dispersion | - | 25 mg | Quartz flask | 300 W Xenon lamp (λ > 420 nm) | 25 mL of TEA: MeOH: $H_2O$ (1:1:1 v/v/v) | - | 3.3 mmol $g^{-1}$ $h^{-1}$ | 5.6@420 nm | [169] |
| PySO-2 | Direct polymer dispersion | - | 10 mg | Flask | 300 W Xenon lamp (λ > 420 nm) | TEOA: $H_2O$ (1:4 v/v) | - | 23.3 mmol $g^{-1}$ $h^{-1}$ | 17.8@420 nm | [170] |
| PBDTTTSOS | Direct polymer dispersion | - | 2 mg | Reaction glass container | 350 W Xenon lamp (λ = 380–780 nm, 1000 W $m^{-2}$) | 10 mL of 1 M AA in NMP: $H_2O$ (1:9 v/v, pH 4) | 3 wt% $H_2PtCl_6$ | 35.7 mmol $g^{-1}$ $h^{-1}$ | 18.9@500 nm | [171] |
| PCz2S-PEG | Direct polymer dispersion | - | 10 mg | Reaction glass container | 350 W Xenon lamp (AM 1.5, λ > 420 nm, 1000 W $m^{-2}$) | 10 mL of TEA: MeOH: $H_2O$ (1:1:1 v/v/v) | 3 wt% $H_2PtCl_6$ | 0.1 mmol $h^{-1}$ | 14.2@420 nm | [172] |
| ICTDB | Direct polymer dispersion | - | 2 mg | Reaction glass container | 350 W Xenon lamp (AM 1.5, λ = 380–780 nm, 1000 W $m^{-2}$) | 10 mL of 1 M AA in NMP: $H_2O$ (1:9 v/v, pH 4) | 3 wt% $H_2PtCl_6$ | 30.0 mmol $g^{-1}$ $h^{-1}$ | 8.4@420 nm | [173] |
| P-BTDO-EDOT | Direct polymer dispersion | - | 10 mg | CEL-SPH2N device | 300 W Xenon lamp (λ > 420 nm) | 100 mL of 0.2 M AA in dimethyl-formamide (DMF): $H_2O$ (1:9 v/v) | - | 87.2 mmol $g^{-1}$ $h^{-1}$ | 8.5@420 nm | [174] |
| F8BT | Nanoprecipitation | PS-PEG-COOH | 16.8 μg $mL^{-1}$ | reaction cuvette | 17 W, 5000 K LED lamp (λ > 420 nm) | 3 mL of 0.2 M aq. AA (pH 4) | - | 8.3 ± 0.2 mmol $g^{-1}$ $h^{-1}$ | 0.5@445 nm | [45] |

**Table 3** (continued)

| Photocatalyst | Fabrication method | Stabilizer | Amount of catalyst | Reactor | Light source | Reaction medium | Co-catalyst | HER | AQY | References |
|---|---|---|---|---|---|---|---|---|---|---|
| PFODTBT | Nanoprecipitation | PS-PEG-COOH | 13 μg $mL^{-1}$ | Sealed cuvette | 17 W, 5000 K LED lamp (λ > 420 nm) | 3 mL of 0.2 M aq. AA (pH 4) | 0.1 wt% residual Pd | 50 ± 0.5 mmol $g^{-1}$ $h^{-1}$ | 0.6@550 nm | [46] |
| PFBT: PFODTBT: ITIC (18:27:55) | Nanoprecipitation | PS-PEG-COOH | 62 μg | 9 mL gas-tight vial | 17 W, 5000 K LED lamp (λ > 420 nm, 500 W $m^{-2}$) | 2 mL of 0.2 M aq. AA (pH 4) | 6 wt% $K_2PtCl_6$ | 60.8 ± 6.7 mmol $g^{-1}$ $h^{-1}$ | 7.0@600 nm | [49] |
| PFODTBT: ITIC (38:62) | Nanoprecipitation | PS-PEG-COOH | 60 μg | 9 mL gas-tight vial | 17 W, 5000 K LED lamp (λ > 420 nm, 500 W $m^{-2}$) | 2 mLa of 0.2 M aq. AA (pH 4) | 6 wt% $K_2PtCl_6$ | 28.0 mmol $g^{-1}$ $h^{-1}$ | 2.1@650 nm | [49] |
| P2c: P3 (1:1) | Nanoprecipitation | - | - | - | 350 W Xenon lamp (λ = 380–780 nm, 1000 W $m^{-2}$) | 10 mL of 0.1 M aq. AA | 3 wt % $H_2PtCl_6$ | 8.9 mmol $g^{-1}$ $h^{-1}$ | - | [65] |
| NDI-BTF | Nanoprecipitation | PS-PEG-COOH | 250 μg | 35 mL reaction glass vessel | 20 W, 6500 K LED lamp (λ > 420 nm, 500 W $m^{-2}$) | 10 mL of 0.1 M aq. AA | 3 wt% $H_2PtCl_6$ | 3.5 mmol $g^{-1}$ $h^{-1}$ | - | [78] |
| PG6 | Nanoprecipitation | Triton | 0.5 mg | 35 mL reaction glass container | 20 W, 6500 K LED lamp (λ > 420 nm, 500 W $m^{-2}$) | 10 mL of 0.1 M aq. AA | 4 wt% $H_2PtCl_6$ | 5.8 mmol $g^{-1}$ $h^{-1}$ | 0.7@460 nm | [104] |
| PITIC-ThF | Nanoprecipitation | - | 5 mg | Reaction glass container | 20 W, 6500 K LED lamp (λ > 420 nm) | 10 mL of 0.1 M aq. AA | 3 wt% $H_2PtCl_6$ | 339.7 mmol $g^{-1}$ $h^{-1}$ | 4.7@700 nm | [109] |

**Table 3** (continued)

| Photocatalyst | Fabrication method | Stabilizer | Amount of catalyst | Reactor | Light source | Reaction medium | Co-catalyst | HER | AQY | References |
|---|---|---|---|---|---|---|---|---|---|---|
| PITIC-ThF | Nanoprecipitation | - | 5 mg | Reaction glass container | Xenon lamp (AM 1.5, λ > 780 nm, 3000 W $m^{-2}$) | 10 mL of 0.1 M aq. AA | 3 wt% $H_2PtCl_6$ | 4.1 mmol $g^{-1}$ $h^{-1}$ | - | [109] |
| PS: PSOS (1:3) | Facile precipitation | - | 0.5 mg | Reaction glass container | 350 W Xenon lamp (λ = 380–780 nm, 1000 W $m^{-2}$) | 10 mL of 1 M AA in NMP: $H_2O$ (1:9 v/v, pH 4) | 3 wt % $H_2PtCl_6$ | 251.2 mmol $g^{-1}$ $h^{-1}$ | 26.2@500 nm | [110] |
| P3HT: $PC_{71}BM$ (1:1) | Nanoprecipitation | $F_4TCNQ$ | 50 μg $mL^{-1}$ | Vial | 93 W LED lamp (1200 W $m^{-2}$) | 2 mL of 0.1 M aq. AA | 5 wt% $H_2PtCl_6$ | - | - | [111] |
| PS-PEG5 | Flash nanoprecipitation | - | 5 mg | Quartz reactor | 300 W Xenon lamp (full-spectrum light irradiation) | 25 mL of 0.2 M aq. AA | 3 wt% Pt | 14.3 mmol $g^{-1}$ $h^{-1}$ | 2.2@405 nm | [175] |
| P10-e | Mini-emulsion polymerization | Sodium dodecyl sulfate (SDS) | 13 μg $mL^{-1}$ | quartz flask | 300 W Xenon lamp (λ > 420 nm) | 25 mL of TEA: MeOH: aqueous (1:1:1 v/v/v, aqueous phase containing water : toluene 9 : 1, SDS 10 mg $mL^{-1}$ and $Na_2CO_3$ 3.5 mg $mL^{-1}$) | 3 wt% $K_2PtCl_6$ | 84.0 mmol $g^{-1}$ $h^{-1}$ | 5.8 ± 0.2@420 nm | [89] |
| PM6:Y6 (7:3) | Mini-emulsion | sodium poly[2-(3-thienyl)-ethoxy-4-butyl-sulfonate] (TEBS) | 1 mg | recirculating batch reactor | solar simulator (AM 1.5G, 1000 W $m^{-2}$) | 12 mL of 0.2 M aq. AA (pH 2.4) | 10 wt% $K_2PtCl_6$ | 0.010 mmol $h^{-1}$ $cm^{-2}$ | 5.0@800 nm | [96] |
| PM6:PCBM (2:8) | Mini-emulsion | TEBS | 1 mg | recirculating batch reactor | solar simulator (AM 1.5G, 1000 W $m^{-2}$) | 12 mL of 0.2 M aq. AA (pH 2.4) | 10 wt% $K_2PtCl_6$ | 0.011 mmol $h^{-1}$ $cm^{-2}$ | 8.7@400 nm | [96] |

**Table 3** (continued)

| Photocatalyst | Fabrication method | Stabilizer | Amount of catalyst | Reactor | Light source | Reaction medium | Co-catalyst | HER | AQY | References |
|---|---|---|---|---|---|---|---|---|---|---|
| PM6:ITCC-M: IDMIC-4 F (1:1.3:0.2) | Micro-emulsion | sodium dodecyl benzene sulfonate (SDBS) | 1.5 mg | - | 300 W Xenon lamp (AM 1.5G, λ = 320–780 nm, 1000 W $m^{-2}$) | 30 mL of 0.2 M aq. AA (pH 2.4) | 10 wt% $K_2PtCl_6$ | 307.0 mmol $g^{-1}$ $h^{-1}$ | 5.9@600 nm | [100] |
| Y6 | Mini-emulsion | TEBS | 0.225 mg | 13 mL liquid batch reactor | 300 W Xenon lamp (1000 W $m^{-2}$) | 3 mL of 0.2 M aq. AA | 2 wt% $K_2PtCl_6$ | 4.2 mmol $g^{-1}$ $h^{-1}$ | 0.05@780 nm | [107] |
| PTB7-Th: EH-IDTBR (3:7) | Mini-emulsion | TEBS | 2 mg | recirculating batch reactor | 300 W Xenon lamp (λ = 350–800 nm) | 20 mL of 0.2 M aq. AA (pH 2) | 5 wt% $K_2PtCl_6$ | 64.0 mmol $g^{-1}$ $h^{-1}$ | 6.2@700 nm | [108] |
| PTB7-Th: EH-IDTBR (3:7) | Mini-emulsion | dodecyltrimethylammonium bromide (DTAB) | 6.67 μg $mL^{-1}$ | recirculating batch reactor | 300 W Xenon lamp (AM 1.5G, λ = 330–1100 nm, 1000 W $m^{-2}$) | 7.5 mL of 0.2 M aq. AA | 24 wt% $K_2PtCl_6$ | 329.3 ± 7.1 mmol $g^{-1}$ $h^{-1}$ | 6.4 ± 0.2 @600 nm | [125] |
| gIDTBT: oIDTBR (1:1) | Mini-emulsion | SDS | 1 mg | recirculating batch reactor | Solar simulator (AM 1.5 G, 1000 W $m^{-2}$) | 12 mL of 0.2 M aq. AA (pH 2) | 10 wt% $K_2PtCl_6$ | 18.5 mmol $g^{-1}$ $h^{-1}$ | 5.3@400 nm | [144] |
| PM6:Y6CO (3:7) | Mini-emulsion | TEBS | 3.33 μg $mL^{-1}$ | recirculating batch reactor | 300 W Xenon lamp (AM 1.5 G, λ = 330–1100 nm, 1000 W $m^{-2}$) | 7.5 mL of 0.2 M aq. AA | 41 wt% $K_2PtCl_6$ | 323.2 mmol $g^{-1}$ $h^{-1}$ | 11.6@700 nm | [149] |

**Table 3** (continued)

| Photocatalyst | Fabrication method | Stabilizer | Amount of catalyst | Reactor | Light source | Reaction medium | Co-catalyst | HER | AQY | References |
|---|---|---|---|---|---|---|---|---|---|---|
| PBDB-T: ITIC (4:6) | Mini-emulsion | SDBS | 1.5 mg | a closed microgas analysis system | 300 W Xenon lamp (AM 1.5, λ = 320–780 nm, 1500 W $m^{-2}$) | 30 mL of 0.2 M aq. AA (pH 3) | 10 wt% $K_2PtCl_6$ | 257.0 mmol $g^{-1}$ $h^{-1}$ | 5.2@650 nm | [176] |
| PM6:TPP (3:7) | Mini-emulsion | TEBS | 2 mg | recirculating batch reactor | 300 W Xenon lamp (AM 1.5G, λ = 330–1100 nm, 1980 W $m^{-2}$) | 30 mL of 0.2 M aq. AA | 20 wt% $K_2PtCl_6$ | 72.8 mmol $g^{-1}$ $h^{-1}$ | 8.6@800 nm | [177] |
| PM6:BTP-2OH (3:7) | Mini-emulsion | TEBS | 1 mg | 45 mL quartz flask | 300 W Xenon lamp (λ = 300–1100 nm) | 12 mL of 0.2 M aq. AA | 15 wt% $K_2PtCl_6$ | 102.1 mmol $g^{-1}$ $h^{-1}$ | 9.2@800 nm | [178] |
| PM6:2FBP-4 F (3:7) | Mini-emulsion | TEBS | 1.67 μg $mL^{-1}$ | recirculating batch reactor | 300 W Xenon lamp (AM 1.5G, λ = 330–1100 nm, 1000 W $m^{-2}$) | 7.5 mL of 0.2 M aq. AA | 24 wt% $K_2PtCl_6$ | 561.8 mmol $g^{-1}$ $h^{-1}$ | 13.9@800 nm | [179] |

Machine learning and high-throughput screening can rapidly navigate the vast chemical and structural space of polymers, predicting candidates with favorable properties for efficient hydrogen evolution [180–182]. When integrated with automated synthesis, these methods may significantly reduce the time from conceptual design to material validation. Moreover, in situ and operando spectroscopies provide critical insights into charge carrier dynamics and interfacial processes under operational conditions—information not accessible through static measurements [183]. These tools will be essential for establishing predictive frameworks and uncovering new principles to guide performance enhancement.

A key future direction lies in advancing polymeric photocatalysts toward practical applications. This will require coupling hydrogen evolution with oxygen evolution to achieve unbiased overall water splitting, a significantly more demanding process than sacrificial systems [184]. In polymeric systems, this challenge is further amplified by the intrinsically limited feasibility of water oxidation and the difficulty of simultaneously satisfying the energetic requirements for both hydrogen and oxygen evolution reactions [185]. Promising strategies include Z-scheme architectures and tandem photocatalytic systems, which offer effective means to manage redox potentials and enable full-cycle water splitting [175, 186]. Such architectures are particularly attractive for polymeric photocatalysts, as they allow spatial or functional separation of redox reactions, thereby enabling independent optimization of the redox processes while maintaining sufficient driving force for both half-reactions. Simultaneously, scaling up necessitates addressing

stability and reproducibility challenges, as well as demonstrating pilot-scale hydrogen production under realistic solar conditions [187]. From a practical standpoint, this will require standardized testing protocols, long-term operation under simulated or natural sunlight, and reproducible performance across scalable or flow-based reactor configurations. Achieving these milestones will be critical to advancing polymeric photocatalysts toward industrial relevance.

## 7 Conclusions

In this review, we have provided an integrated overview of the strategies and mechanisms governing polymeric photocatalysts for solar-driven hydrogen evolution. Molecular-level engineering, encompassing backbone design, side-chain modification, and heteroatom incorporation, has enabled systematic control over key parameters such as optical properties, charge-carrier dynamics, and surface chemistry, thereby enhancing intrinsic photocatalytic activity. Complementing these efforts, particle-level engineering has emerged as a powerful approach to improve dispersibility, water compatibility, and interfacial charge transfer by modulating particle size, morphology, and molecular ordering. These advances have been further supported by diverse fabrication methods, including direct polymer dispersion, nanoprecipitation, mini-emulsion processing, and surfactant-free approaches, each offering distinct advantages for constructing well-defined polymer architectures.

Photophysical investigations, including steady-state and time-resolved spectroscopy, transient absorption, and PIAS, have further elucidated the relationships between polymer structure, charge-carrier behavior, and catalytic performance. Collectively, these studies provide critical mechanistic insight into exciton generation, charge separation, transport, interfacial extraction, and proton reduction. Despite this progress, substantial challenges remain, particularly in establishing standardized evaluation protocols for hydrogen evolution performance, enhancing long-term stability, and achieving unbiased overall water splitting without SAs. Overcoming these obstacles will require deeper integration of molecular design, interfacial engineering, and operando characterization under realistic reaction conditions.

Looking ahead, the convergence of high-throughput experimentation, machine learning-guided materials discovery, and advanced spectroscopic techniques presents promising pathways to accelerate innovation. Continued efforts to unify design, fabrication, and mechanistic understanding will be essential for realizing the full potential of polymeric photocatalysts and advancing their deployment in practical solar-to-hydrogen technologies.

**Acknowledgements**
This work was supported by the National Research Foundation of Korea (NRF) grant funded by the Korea government (MSIT) (RS-2024-00438426 and RS-2023-00213920).

**Author contributions**
SK was responsible for the conceptualization of the review, conducted the comprehensive literature survey, drafted the manuscript, and prepared the figures and tables. MK contributed to the literature investigation and assisted in the preparation of the figures. DL and Prof. LS offered conceptual guidance, and contributed substantial revisions to the manuscript. GH, CP, and DL assisted in the literature review. Prof. HC oversaw the overall preparation of the manuscript and provided comprehensive guidance throughout its development. All authors read and approved the final version of the manuscript.

**Funding**
The funders had no involvement in the conceptualization of this review, the literature survey and interpretation, nor in the drafting or revision of the manuscript.

**Data availability**
This review did not generate or analyze any new datasets. All data and materials referenced herein are obtained from previously published studies and publicly available scientific literature.

## Declarations

**Competing interests**
The authors declare that they have no competing interests.

**Author details**
[1]School of Energy Engineering, Kyungpook National University, Daegu 41566, Republic of Korea
[2]Department of Chemistry, University of Oxford, 12 Mansfield Road, Oxford OX1 3TA, UK

Received: 11 December 2025 / Accepted: 9 February 2026
Published online: 16 February 2026

**References**

1. E.D. Coyle, W. Grimson, B. Basu, M. Murphy, in *Understanding the Global Energy Crisis*, ed. E.D. Coyle, R.A. Simmons (Purdue University Press, West Lafayette, 2014), p. 11. https://doi.org/10.2307/j.ctt6wq56p
2. M. Höök, X. Tang, Depletion of fossil fuels and anthropogenic climate change—A review. Energy Policy **52**, 797–809 (2013). https://doi.org/10.1016/j.enpol.2012.10.046
3. H. Feng, The impact of renewable energy on carbon neutrality for the sustainable environment: role of green finance and technology innovations. Front. Environ. Sci. **10**, 924857 (2022). https://doi.org/10.3389/fenvs.2022.924857
4. 4. UNFCCC, Paris agreement (2015). https://unfccc.int/documents/9064. Accessed 9 Dec 2025
5. N. Kannan, D. Vakeesan, Solar energy for future world: a review. Renew. Sustain. Energy Rev. **62**, 1092–1105 (2016). https://doi.org/10.1016/j.rser.2016.05.022
6. N.S. Lewis, D.G. Nocera, Powering the planet: Chemical challenges in solar energy utilization. Proc. Natl. Acad. Sci. USA **103**, 15729–15735 (2006). https://doi.org/10.1073/pnas.0603395103
7. J. Jia, L.C. Seitz, J.D. Benck, Y. Huo, Y. Chen, J.W.D. Ng, T. Bilir, J.S. Harris, T.F. Jaramillo, Solar water splitting by photovoltaic-electrolysis with a solar-to-hydrogen efficiency over 30%. Nat. Commun. **7**, 13237 (2016). https://doi.org/10.1038/ncomms13237
8. L. Yao, N. Guijarro, F. Boudoire, Y. Liu, A. Rahmanudin, R.A. Wells, A. Sekar, H.H. Cho, J.H. Yum, F.L. Formal, K. Sivula, Establishing stability in organic semiconductor photocathodes for solar hydrogen production. J. Am. Chem. Soc. **142**, 7795–7802 (2020). https://pubs.acs.org/doi/ https://doi.org/10.1021/jacs.0c00126

9. H.H. Cho, L. Yao, J.H. Yum, Y. Liu, F. Boudoire, R.A. Wells, N. Guijarro, A. Sekar, K. Sivula, A semiconducting polymer bulk heterojunction photoanode for solar water oxidation. Nat. Catal. **4**, 431–438 (2021). https://doi.org/10.1038/s41929-021-00617-x
10. K. Maeda, K. Teramura, D. Lu, T. Takata, N. Saito, Y. Inoue, K. Domen, Photocatalyst releasing hydrogen from water. Nature **440**, 295 (2006). https://doi.org/10.1038/440295a
11. J. He, C. Janáky, Recent advances in solar-driven carbon dioxide conversion: expectations versus reality. ACS Energy Lett. **5**, 1996–2014 (2020). https://pubs.acs.org/doi/ https://doi.org/10.1021/acsenergylett.0c00645
12. J. Choi, W. Jung, S. Gonzlez-Carrero, J.R. Durrant, H. Cha, T. Park, Understanding charge carrier dynamics in organic photocatalysts for hydrogen evolution. Energy Environ. Sci. **17**, 7999–8018 (2024). https://doi.org/10.1039/D4EE01808G
13. H. Zhao, Z.Y. Yuan, Progress and perspectives for solar-driven water electrolysis to produce green hydrogen. Adv. Energy Mater. **13**, 2300254 (2023). https://doi.org/10.1002/aenm.202300254
14. M. Grätzel, Photoelectrochemical cells. Nature **414**, 338–344 (2001). https://doi.org/10.1038/35104607
15. A. Vilanova, P. Dias, T. Lopes, A. Mendes, The route for commercial photoelectrochemical water splitting: a review of large-area devices and key upscaling challenges. Chem. Soc. Rev. **53**, 2388–2434 (2024). https://doi.org/10.1039/D1CS01069G
16. L. Steier, S. Holliday, A bright outlook on organic photoelectrochemical cells for water splitting. J. Mater. Chem. A **6**, 21809–21826 (2018). https://doi.org/10.1039/C8TA07036A
17. L. Clarizia, M.N. Nadagouda, D.D. Dionysiou, Recent advances and challenges of photoelectrochemical cells for hydrogen production. Curr. Opin. Green Sustain. Chem. **41**, 100825 (2023). https://doi.org/10.1016/j.cogsc.2023.100825
18. A. Paracchino, V. Laporte, K. Sivula, Highly active oxide photocathode for photoelectrochemical water reduction. Nat. Mater. **10**, 456–461 (2011). https://doi.org/10.1038/nmat3017
19. C.S. Gopinath, N. Nalajala, A scalable and thin film approach for solar hydrogen generation: a review on enhanced photocatalytic water splitting. J. Mater. Chem. A **9**, 1353–1371 (2021). https://doi.org/10.1039/D0TA09619A
20. K.T. Møller, T.R. Jensen, E. Akiba, H.-W. Li, Hydrogen-A sustainable energy carrier. Prog Nat. Sci. Mater. Int. **27**, 34–40 (2017). https://doi.org/10.1016/j.pnsc.2016.12.014
21. S. Nishioka, F.E. Osterloh, X. Wang, T.E. Mallouk, K. Maeda, Photocatalytic water splitting. Nat. Rev. Methods Prim. **3**, 42 (2023). https://doi.org/10.1038/s43586-023-00226-x
22. B.P. Mishra, J. dahiya, V. Krishnan, Semiconductor photocatalysts for hydrogen evolution: critical role of cocatalysts in enhancing performance. Chem. Commun. **61**, 17302–17329 (2025). https://doi.org/10.1039/D5CC04459F
23. N.M. Gupta, Factors affecting the efficiency of a water splitting photocatalyst: a perspective. Renew. Sustain. Energy Rev. **71**, 585–601 (2017). https://doi.org/10.1016/j.rser.2016.12.086
24. K. Takanabe, Photocatalytic water splitting: quantitative approaches toward photocatalyst by design. ACS Catal. **7**, 8006–8022 (2017). https://pubs.acs.org/doi/ https://doi.org/10.1021/acscatal.7b02662
25. Y. Deng, Y. Shi, L. Li, R. Tang, Z. Zhou, S. Xiong, W. Li, J. Liu, Y. Huang, Molecular modification: a promising strategy for the design of donor-acceptor-type organic polymers photocatalyst. Appl. Catal. B **352**, 124043 (2024). https://doi.org/10.1016/j.apcatb.2024.124043
26. R.S. Kangutkar, P. Walko, P.L. Dhepe, G.P. Nayaka, J. Manjanna, Photocatalytic hydrogen evolution by $MoO_3$@*g*-$C_3N_4$ and $MoO_3$@*f*-MWCNT nanocomposites in deionized and natural seawater under visible light. ACS Appl. Nano Mater. **8**, 7175–7189 (2025). https://pubs.acs.org/doi/ https://doi.org/10.1021/acsanm.5c00297
27. X. Wang, B. Liu, S. Ma, Y. Zhang, L. Wang, G. Zhu, W. Huang, S. Wang, Induced dipole moments in amorphous ZnCdS catalysts facilitate photocatalytic $H_2$ evolution. Nat. Commun. **15**, 2600 (2024). https://doi.org/10.1038/s41467-024-47022-z
28. D. Zhao, Y. Wang, C.L. Dong, Y.C. Huang, J. Chen, F. Xue, S. Shen, L. Guo, Boron-doped nitrogen-deficient carbon nitride-based Z-scheme heterostructures for photocatalytic overall water splitting. Nat. Energy **6**, 388–397 (2021). https://doi.org/10.1038/s41560-021-00795-9
29. A. Fujishima, K. Honda, Electrochemical photolysis of water at a semiconductor electrode. Nature **238**, 37–38 (1972). https://doi.org/10.1038/238037a0
30. M. Matsumura, S. Furukawa, Y. Saho, H. Tsubomura, Cadmium sulfide photocatalyzed hydrogen production from aqueous solutions of sulfite: effect of crystal structure and preparation method of the catalyst. J. Phys. Chem. **89**, 1327–1329 (1985). https://doi.org/10.1021/j100254a001
31. Y.P. Xie, Z.B. Yu, G. Liu, X.L. Ma, H.M. Cheng, CdS–mesoporous ZnS core–shell particles for efficient and stable photocatalytic hydrogen evolution under visible light. Energy Environ. Sci. **7**, 1895–1901 (2014). https://doi.org/10.1039/C3EE43750G
32. Z. Chen, T.T. Fan, X. Yu, Q.L. Wu, Q.H. Zhu, L.Z. Zhang, J.H. Li, W.P. Fang, X.D. Yi, Gradual carbon doping of graphitic carbon nitride towards metal-free visible light photocatalytic hydrogen evolution. J. Mater. Chem. A **6**, 15310–15319 (2018). https://doi.org/10.1039/C8TA03303J
33. M. Batzill, Fundamental aspects of surface engineering of transition metal oxide photocatalysts. Energy Environ. Sci. **4**, 3275–3286 (2011). https://doi.org/10.1039/C1EE01577J
34. I. Ullah, M. Amin, P. Zhao, N. Qin, A.W. Xu, Recent advances in inorganic oxide semiconductor-based S-scheme heterojunctions for photocatalytic hydrogen evolution. Inorg. Chem. Front. **12**, 1329–1348 (2025). https://doi.org/10.1039/D4QI02797C
35. R.R. Xu, Q. Su, in *Modern Inorganic Synthetic Chemistry*, ed. R. Xu, Y. Xu (Elsevier, Amsterdam, 2017), p. 9. https://doi.org/10.1016/B978-0-444-63591-4.00002-1
36. DB Mitzi (ed.), in *Solution Processing of Inorganic Materials* (Wiley, Hoboken, 2008). https://doi.org/10.1002/9780470407790
37. K. Villa, J.R. Galán-Mascarós, N. López, E. Palomares, Photocatalytic water splitting: advantages and challenges. Sustain. Energy Fuels **5**, 4560–4569 (2021). https://doi.org/10.1039/D1SE00808K
38. M.B. Hasan, M.M. Parvez, A.Y. Abir, M.F. Ahmad, A review on conducting organic polymers: concepts, applications, and potential environmental benefits. Heliyon **11**, e42375 (2025). https://doi.org/10.1016/j.heliyon.2025.e42375
39. N. Luo, P. Ren, Y. Feng, X. Shao, H.-L. Zhang, Z. Liu, Side-chain engineering of conjugated polymers for high-performance organic field-effect transistors. J. Phys. Chem. Lett. **13**, 1131–1146 (2022). https://pubs.acs.org/doi/ https://doi.org/10.1021/acs.jpclett.1c03909
40. Y. Guo, Q. Zhou, B. Zhu, C.Y. Tang, Y. Zhu, Advances in organic semiconductors for photocatalytic hydrogen evolution reaction. EES Catal. **1**, 333–352 (2023). https://doi.org/10.1039/D3EY00047H
41. S. Yanagida, A. Kabumoto, K. Mizumoto, C. Pac, K. Yoshino, Poly(*p*-phenylene)-catalysed photoreduction of water to hydrogen. J. Chem. Soc. Chem. Commun. 474–475 (1985). https://doi.org/10.1039/C39850000474
42. T. Shibata, A. Kabumoto, T. Shiragami, O. Ishitani, C. Pac, S. Yanagida, Novel visible-light-driven photocatalyst. Poly(p-phenylene)-catalyzed photoreductions of water, carbonyl compounds, and olefins. J. Phys. Chem. **94**, 2068–2076 (1990). https://pubs.acs.org https://doi.org/10.1021/j100368a063
43. M. Sachs, R.S. Sprick, D. Pearce, S.A.J. Hillman, A. Monti, A.A.Y. Guilbert, N.J. Brownbill, S. Dimitrov, X. Shi, F. Blanc, M.A. Zwijnenburg, J. Nelson, J.R. Durrant, A.I. Cooper, Understanding structure-activity relationships in linear polymer photocatalysts for hydrogen evolution. Nat. Commun. **9**, 4968 (2018). https://doi.org/10.1038/s41467-018-07420-6
44. G. Shu, Y. Li, Z. Wang, J.X. Jiang, F. Wang, Poly(dibenzothiophene-S,S-dioxide) with visible light-induced hydrogen evolution rate up to 44.2 mmol $h^{-1}$ $g^{-1}$ promoted by $K_2HPO_4$. Appl. Catal. B **261**, 118230 (2020). https://doi.org/10.1016/j.apcatb.2019.118230
45. L. Wang, R. Fernández-Terán, L. Zhang, D.L.A. Fernandes, L. Tian, H. Chen, H. Tian, Organic polymer dots as photocatalysts for visible light-driven hydrogen generation. Angew Chem. Int. Ed. **55**, 12306–12310 (2016). https://doi.org/10.1002/anie.201607018
46. P.B. Pati, G. Damas, L. Tian, D.L.A. Fernandes, L. Zhang, I.B. Pehlivan, T. Edvinsson, C.M. Araujo, H. Tian, An experimental and theoretical study of an efficient polymer nano-photocatalyst for hydrogen evolution. Energy Environ. Sci. **10**, 1372–1376 (2017). https://doi.org/10.1039/C7EE00751E
47. M. Axelsson, C.F.N. Marchiori, P. Huang, C.M. Araujo, H. Tian, Small organic molecule based on benzothiadiazole for electrocatalytic hydrogen production. J. Am. Chem. Soc. **143**, 21229–21233 (2021). https://pubs.acs.org/doi/ https://doi.org/10.1021/jacs.1c10600
48. M. Axelsson, Z. Xia, S. Wang, M. Cheng, H. Tian, Role of the benzothiadiazole unit in organic polymers on photocatalytic hydrogen production. JACS Au **4**, 570–577 (2024). https://pubs.acs.org/doi/ https://doi.org/10.1021/jacsau.3c00681
49. A. Liu, L. Gedda, M. Axelsson, M. Pavliuk, K. Edwards, L. Hammarström, H. Tian, Panchromatic ternary polymer dots involving sub-picosecond energy and charge transfer for efficient and stable photocatalytic hydrogen evolution. J. Am. Chem. Soc. **143**, 2875–2885 (2021). https://pubs.acs.org/doi/ https://doi.org/10.1021/jacs.0c12654

50. M.H. Elsayed, M. Abdellah, Y.H. Hung, J. Jayakumar, L.Y. Ting, A.M. Elewa, C.L. Chang, W.C. Lin, K.L. Wang, M. Abdel-Hafiez, H.W. Hung, M. Horie, H.H. Chou, Hydrophobic and hydrophilic conjugated polymer dots as binary photocatalysts for enhanced visible-light-driven hydrogen evolution through Förster resonance energy transfer. ACS Appl. Mater. Interfaces **13**, 56554–56565 (2021). https://doi.org/10.1021/acsami.1c15812
51. A. Liu, S. Wang, H. Song, Y. Liu, L. Gedda, K. Edwards, L. Hammarström, H. Tian, Excited-state and charge-carrier dynamics in binary conjugated polymer dots towards efficient photocatalytic hydrogen evolution. Phys. Chem. Chem. Phys. **25**, 2935–2945 (2023). https://doi.org/10.1039/D2CP04204E
52. S. Kashani, J.J. Rech, T. Liu, K. Baustert, A. Ghaffari, I. Angunawela, Y. Xiong, A. Dinku, W. You, K. Graham, H. Ade, Exciton binding energy in organic polymers: experimental considerations and tuning prospects. Adv. Energy Mater. **14**, 2302837 (2023). https://doi.org/10.1002/aenm.202302837
53. Y. Wang, A. Vogel, M. Sachs, R.S. Sprick, L. Willbraham, S.J.A. Moniz, R. Godin, M.A. Zwijnenburg, J.R. Durrant, A.I. Cooper, J. Tang, Current Understanding and challenges of solar-driven hydrogen generation using polymeric photocatalysts. Nat. Energy **4**, 746–760 (2019). https://doi.org/10.1038/s41560-019-0456-5
54. J. Kosco, I. McCulloch, Residual Pd enables photocatalytic $H_2$ evolution from conjugated polymers. ACS Energy Lett. **3**, 2846–2850 (2018). https://doi.org/10.1021/acsenergylett.8b01853
55. M. Sachs, H. Cha, J. Kosco, C.M. Aitchison, L. Francas, S. Corby, C.L. Chiang, A.A. Wilson, R. Godin, A. Fahey-Williams, A.I. Cooper, R.S. Sprick, I. McCulloch, J.R. Durrant, Tracking charge transfer to residual metal clusters in conjugated polymers for photocatalytic hydrogen evolution. J. Am. Chem. Soc. **142**, 14574–14587 (2020). https://doi.org/10.1021/jacs.0c06104
56. D. Meng, X. Ruan, M. Xu, D. Jiao, G. Fang, Y. Qiu, Y. Zhang, H. Zhang, S.K. Ravi, X. Cui, An S-scheme artificial photosynthetic system with H-$TiO_2$/g-$C_3N_4$ heterojunction coupled with MXene boosts solar $H_2$ evolution. J. Mater. Sci. Technol. **211**, 22–29 (2025). https://doi.org/10.1016/j.jmst.2024.05.047
57. L. Fan, J. Han, K. Wei, C. Ma, S. Feng, Y. Zhou, X. Dai, Z. Ye, Y. Wang, Mn-doped CdS/$Cu_2O$: an S-scheme heterojunction for photocatalytic hydrogen production. J. Alloys Compd. **960**, 170382 (2023). https://doi.org/10.1016/j.jallcom.2023.170382
58. Y. Hao, J. Zhao, H. Li, M. Li, G. Guo, J. Zhang, F. Fu, Side chain engineering for modulating hydrophilicity of benzobisthiazole-based linear conjugated polymer to improve the photocatalytic hydrogen evolution. J. Photochem. Photobiol. A **469**, 116530 (2025). https://doi.org/10.1016/j.jphotochem.2025.116530
59. Z. Huang, Y. Wu, C. Yu, Z. Wang, C. Jin, Z. Li, S. Yin, Impact of the donor–acceptor structure on photocatalytic hydrogen generation by polyfluorene polymer dots. ACS Appl. Polym. Mater. **7**, 3399–3408 (2025). https://pubs.acs.org/doi/ https://doi.org/10.1021/acsapm.5c00214
60. T.F. Huang, K.J. Lin, Y.R. Zhuang, Y.E. Sun, H.H. Chou, Flexible, nonfused sulfone functionalized polymer with enhanced active site access for photocatalytic sacrificial hydrogen evolution. Sci. Adv. **11**, eadx1629 (2025). https://doi.org/10.1126/sciadv.adx1629
61. W.C. Lin, Y.H. Wu, Y.E. Sun, M.M. Elsenety, W.C. Lin, J.C. Yen, H.K. Hsu, B.H. Chen, H.Y. Huang, C.A. Chang, T.F. Huang, Y.R. Zhuang, Y.T. Tseng, K.H. Lin, S.D. Yang, C.H. Yu, H.H. Chou, Symmetry-breaking of Dibenzo[b,d]thiophene sulfone enhancing Polaron generation for boosted photocatalytic hydrogen evolution. Angew Chem. **136**, e202407702 (2024). https://doi.org/10.1002/ange.202407702
62. J. Zhan, X. Zhang, C. Zhang, Y. Yang, X. Ding, D. Ding, B. Chai, K. Dai, H. Chen, Thienyl-fused dibenzothiophene-S,S-dioxide based conjugated polymer toward highly efficient photocatalytic hydrogen production. Int. J. Hydrog. Energy **80**, 115–124 (2024). https://doi.org/10.1016/j.ijhydene.2024.07.001
63. A. Holmes, J. Pan, L. Wang, L. Franco, R.R. Bicudo, B. Albinsson, C.M. Araujo, W. Zhu, D. Wang, T.Q. Nguyen, J. Zhu, E. Wang, Highly efficient platinum-free photocatalytic hydrogen evolution from low-cost conjugated polymer nanoparticles. Adv. Mater. **37**, 2507702 (2025). https://doi.org/10.1002/adma.202507702
64. A. Liu, C.W. Tai, K. Holá, H. Tian, Hollow polymer dots: nature-mimicking architecture for efficient photocatalytic hydrogen evolution reaction. J. Mater. Chem. A **7**, 4797–4803 (2019). https://doi.org/10.1039/C8TA12146J
65. K.D.G. Huynh, Y.T. Huang, M.C. Tsai, I.M.A. Mekhemer, J. Jayakumar, Y.T. Lin, C.H. Li, S. Pratihar, T.F. Huang, D.C.K. Hoang, S.D. Yang, H.H. Chou, M. Horie, Boosting photocatalytic hydrogen evolution from binary mixture of hydrophilic-hydrophobic conjugated polymer dots with variable saponification degrees and molecular weights. Chem. Eng. J. **509**, 161082 (2025). https://doi.org/10.1016/j.cej.2025.161082
66. S.A.J. Hillman, R.S. Sprick, D. Pearce, D.J. Woods, Y.Y. Sit, X. Shi, A.I. Cooper, J.R. Durrant, J. Nelson, Why do sulfone-containing polymer photocatalysts work so well for sacrificial hydrogen evolution from water? J. Am. Chem. Soc. **144**, 19382–19395 (2022). https://pubs.acs.org/doi/ https://doi.org/10.1021/jacs.2c07103
67. J. Johnston, C. O'Rourke, A. Mills, Photo-induced absorption spectroscopy (PIAS) study of the kinetics of water oxidation by P25 $TiO_2$ using periodate as an electron acceptor. Appl. Catal. Gen. **644**, 118817 (2022). https://doi.org/10.1016/j.apcata.2022.118817
68. S. Jadoun, D.S. Rathore, U. Riaz, N.P.S. Chauhan, Tailoring of conducting polymers via copolymerization–A review. Eur. Polym. J. **155**, 110561 (2021). https://doi.org/10.1016/j.eurpolymj.2021.110561
69. R.S. Sprick, C.M. Aitchison, E. Berardo, L. Turcani, L. Willbraham, B.M. Alston, K.E. Jelfs, M.A. Zwijnenburg, A.I. Cooper, Maximising the hydrogen evolution activity in organic photocatalysts by co-polymerisation. J. Mater. Chem. A **6**, 11994–12003 (2018). https://doi.org/10.1039/C8TA04186E
70. R.S. Sprick, B. Bonillo, R. Clowes, P. Guiglion, N.J. Brownbill, B.J. Slater, F. Blanc, M.A. Zwijnenburg, D.J. Adams, A.I. Cooper, Visible-light-driven hydrogen evolution using planarized conjugated polymer photocatalysts. Angew Chem. Int. Ed. **55**, 1792–1796 (2015). https://doi.org/10.1002/anie.201510542
71. C. Bai, B. Liu, Conjugated polymers for visible-light-driven photocatalysis. Energy Environ. Sci. **13**, 24–52 (2020). https://doi.org/10.1039/C9EE01935A
72. C. Yang, B. Cheng, J. Xu, J. Yu, S. Cao, Donor-acceptor-based conjugated polymers for photocatalytic energy conversion. EnergyChem **6**, 100116 (2024). https://doi.org/10.1016/j.enchem.2023.100116
73. Z.A. Lan, W. Ren, X. Chen, Y. Zhang, X. Wang, Conjugated donor-acceptor polymer photocatalysts with electron-output tentacles for efficient hydrogen evolution. Appl. Catal. B **245**, 596–603 (2019). https://doi.org/10.1016/j.apcatb.2019.01.010
74. Z.A. Lan, M. Wu, Z. Fang, X. Chi, X. Chen, Y. Zhang, X. Wang, A fully coplanar donor–acceptor polymeric semiconductor with promoted charge separation kinetics for photochemistry. Angew Chem. Int. Ed. **60**, 16355–16359 (2021). https://doi.org/10.1002/anie.202103992
75. C. Ru, T. Zhou, J. Zhang, X. Wu, P. Sun, P. Chen, L. Zhou, H. Zhao, J. Wu, X. Pan, Introducing secondary acceptors into conjugated polymers to improve photocatalytic hydrogen evolution. Macromolecules **54**, 8839–8848 (2021). https://doi.org/10.1021/acs.macromol.1c00705
76. N. Liu, S. Xie, Y. Huang, J. Lu, H. Shi, S. Xu, G. Zhang, X. Chen, Dual–acceptor engineering in pyrene-based covalent organic frameworks for boosting photocatalytic hydrogen evolution. Adv. Energy Mater. **14**, 2402395 (2024). https://doi.org/10.1002/aenm.202402395
77. W.C. Lin, J. Jayakumar, C.L. Chang, L.Y. Ting, T.F. Huang, M.H. Elsayed, A.M. Elewa, Y.T. Lin, J.J. Liu, Y.T. Tseng, H.H. Chou, Sulfide oxidation tuning in 4,8-bis(5-(2-ethylhexyl)thiophen-2-yl)benzo[1,2-*b*:4,5-*b'*]dithiophene based dual acceptor copolymers for highly efficient photocatalytic hydrogen evolution. J. Mater. Chem. A **10**, 6641–6648 (2022). https://doi.org/10.1039/D2TA00241H
78. I.M.A. Mekhemer, Y.S. Wu, A.M. Elewa, W.C. Chen, C.C. Chueh, H.H. Chou, Naphthalenediimide-Based polymer Dots with dual acceptors as a new class of photocatalysts for photocatalytic hydrogen generation under visible light irradiation. Solar RRL **8**, 2300994 (2024). https://doi.org/10.1002/solr.202300994
79. Q. Dai, X. Lang, J.L. Brédas, T. Wang, Q. Jiang, Impact of the alkyl side-chain length on solubility, interchain packing, and charge-transport properties of amorphous π-conjugated polymers. Moore More **1**, 8 (2024). https://doi.org/10.1007/s44275-024-00008-x
80. D.J. Woods, R.S. Sprick, C.L. Smith, A.J. Cowan, A.I. Cooper, A solution-processable polymer photocatalyst for hydrogen evolution from water. Adv. Energy Mater. **7**, 1700479 (2017). https://doi.org/10.1002/aenm.201700479
81. B. Meng, J. Liu, L. Wang, Oligo(ethylene glycol) as side chains of conjugated polymers for optoelectronic applications. Polym. Chem. **11**, 1261–1270 (2020). https://doi.org/10.1039/C9PY01469A
82. D.J. Woods, S.A.J. Hillman, D. Pearce, L. Willbraham, L.Q. Flagg, W. Duffy, I. McCulloch, J.R. Durrant, A.A.Y. Guillbert, M.A. Zwijnenburg, R.S. Sprick, J. Nelson, A.I. Cooper, Side-chain tuning in conjugated polymer photocatalysts for improved hydrogen production from water. Energy Environ. Sci. **13**, 1843–1855 (2020). https://doi.org/10.1039/D0EE01213K
83. Y. Bai, D.J. Woods, L. Willbraham, C.M. Aitchison, M.A. Zwijnenburg, R.S. Sprick, A.I. Cooper, Hydrogen evolution from water using heteroatom substituted fluorene conjugated co-polymers. J. Mater. Chem. A **8**, 8700–8705 (2020). https://doi.org/10.1039/D0TA02599B

84. Y. Liu, H. Yu, C. Shi, Z. Xiang, Localized electron density modulation in conjugated polymer nanosheets for boosting photocatalytic $H_2$ evolution. J. Mater. Chem. A **9**, 19625–19630 (2021). https://doi.org/10.1039/D1TA02193A
85. A.M. Elewa, A.F.M. EL-Mahdy, M.H. Elsayed, M.G. Mohamed, S.W. Kuo, H.H. Chou, Sulfur-doped triazine-conjugated microporous polymers for achieving the robust visible-light-driven hydrogen evolution. Chem. Eng. J. **421**, 129825 (2021). https://doi.org/10.1016/j.cej.2021.129825
86. Y. Xiang, X. Wang, L. Rao, P. Wang, D. Huang, X. Ding, X. Zhang, S. Wang, H. Chen, Y. Zhu, Conjugated polymers with sequential fluorination for enhanced photocatalytic $H_2$ evolution via proton-coupled electron transfer. ACS Energy Lett. **3**, 2544–2549 (2018). https://pubs.acs.org/doi/ https://doi.org/10.1021/acsenergylett.8b01535
87. R.J. Lyons, R.S. Sprick, Processing polymer photocatalysts for photocatalytic hydrogen evolution. Mater. Horiz. **11**, 3764–3791 (2024). https://doi.org/10.1039/D4MH00482E
88. Y. Jia, Y. Liang, Y. Yan, Y. Lin, C. Zhang, Size-dependent hydrogen evolution in organic photovoltaic catalysts: balancing exciton dissociation and charge transport. Nanoscale **17**, 17711–17718 (2025). https://doi.org/10.1039/D5NR01436K
89. C.M. Aitchison, R.S. Sprick, A.I. Cooper, Emulsion polymerization derived organic photocatalysts for improved light-driven hydrogen evolution. J. Mater. Chem. A **7**, 2490–2496 (2019). https://doi.org/10.1039/C8TA11383A
90. R.S. Sprick, Y. Bai, A.A.Y. Guilbert, M. Zbiri, C.M. Aitchison, L. Willbraham, Y. Yan, D.J. Woods, M.A. Zwijnenburg, A.I. Cooper, Photocatalytic hydrogen evolution from water using fluorene and dibenzothiophene sulfone-conjugated microporous and linear polymers. Chem. Mater. **31**, 305–313 (2019). https://pubs.acs.org/doi/ https://doi.org/10.1021/acs.chemmater.8b02833
91. S. Kim, X. Zhou, Y. Li, Q. Yang, X. Liu, R. Graf, P.W.M. Blom, C.T.J. Ferguson, K. Landfester, Size-Dependent photocatalytic reactivity of conjugated microporous polymer nanoparticles. Adv. Mater. **36**, 2404054 (2024). https://doi.org/10.1002/adma.202404054
92. P.R. Sajanlal, T.S. Sreeprasad, A.K. Samal, T. Pradeep, Anisotropic nanomaterials: structure, growth, assembly, and functions. Nano Rev. **2**, 5883 (2011). https://doi.org/10.3402/nano.v2i0.5883
93. Q. Gong, J. Luo, C. Meng, Z. Xiong, S. Zhang, T. Yu, Anisotropic photoelectric properties of aligned P3HT nanowire arrays fabricated via solution blade coating and UV-induced molecular ordering. Materials **18**, 2649 (2025). https://doi.org/10.3390/ma18112649
94. R. Bariki, R.G. Joseph, O.M. El-Kadri, M.H. Al-Sayah, The development of metal-free porous organic polymers for sustainable carbon dioxide photoreduction. Nanomaterials **14**, 1432 (2024). https://doi.org/10.3390/nano14171432
95. N.P. Holmes, S. Chambon, A. Holmes, X. Xu, K. Hirakawa, E. Deniau, C. Lartigau-Dagron, A. Bousquet, Organic semiconductor colloids: from the knowledge acquired in photovoltaics to the generation of solar hydrogen fuel. Curr. Opin. Colloid Interface Sci. **56**, 101511 (2021). https://doi.org/10.1016/j.cocis.2021.101511
96. J. Kosco, S. Gonzalez-Carrero, C.T. Howells, T. Fei, Y. Dong, R. Sougrat, G.T. Harrison, Y. Firdaus, R. Sheelamanthula, B. Purushothaman, F. Moruzzi, W. Xu, L. Zhao, A. Basu, S.D. Wolf, T.D. Anthopoulos, J.R. Durrant, I. McCulloch, Generation of long-lived charges in organic semiconductor heterojunction nanoparticles for efficient photocatalytic hydrogen evolution. Nat. Energy **7**, 340–351 (2022). https://doi.org/10.1038/s41560-022-00990-2
97. O.P. Dimitriev, D.A. Blank, C. Ganser, C. Teichert, Effect of the polymer chain arrangement on exciton and Polaron dynamics in P3HT and P3HT:PCBM films. J. Phys. Chem. C **122**, 17096–17109 (2018). https://pubs.acs.org/doi/ https://doi.org/10.1021/acs.jpcc.8b05155
98. Q. shi, H. Chen, Y. Wang, R. Wang, J. Xu, C. Zheng, Amorphous solid dispersions: role of the polymer and its importance in physical stability and in vitro performance. Pharmaceutics **14**, 1747 (2022). https://doi.org/10.3390/pharmaceutics14081747
99. H. Wang, X. Sun, D. Li, X. Zhang, S. Chen, W. Shao, Y. Tian, Y. Xie, Boosting Hot-Electron generation: exciton dissociation at the order–disorder interfaces in polymeric photocatalysts. J. Am. Chem. Soc. **139**, 2468–2473 (2017). https://doi.org/10.1021/jacs.6b12878
100. Y. Yang, D. Li, J. Cai, H. Wang, C. Guo, S. Wen, W. Li, T. Wang, D. Liu, Enhanced photocatalytic hydrogen evolution from organic ternary heterojunction nanoparticles featuring a compact alloy-like phase. Adv. Funct. Mater. **33**, 2209643 (2022). https://doi.org/10.1002/adfm.202209643
101. S. Deng, L. Li, J. Zhang, Y. Wang, Z. Huang, H. Chen, Semiconducting polymer dots for point-of-care biosensing and in vivo bioimaging: a concise review. Biosensors **13**, 137 (2023). https://doi.org/10.3390/bios13010137
102. M.V. Pavliuk, S. Wrede, A. Liu, A. Brnovic, S. Wang, M. Axelsson, H. Tian, Preparation, characterization, evaluation and mechanistic study of organic polymer nano-photocatalysts for solar fuel production. Chem. Soc. Rev. **51**, 6909–6935 (2022). https://doi.org/10.1039/D2CS00356B
103. M. Kuddushi, C. Kanike, B.B. Xu, X. Zhang, Recent advances in nanoprecipitation: from mechanistic insights to applications in nanomaterial synthesis. Soft Matter **21**, 2759–2781 (2025). https://doi.org/10.1039/D5SM00006H
104. A.M. Elewa, C.Y. Liao, W.L. Li, I.M.A. Mekhemer, H.H. Chou, Benzo[*d*][1,2,3] thiadiazole-based polymer dots as photocatalysts for enhanced efficiency and stability of photocatalytic hydrogen evolution under visible light irradiation. Macromolecules **56**, 1352–1361 (2023). https://pubs.acs.org/doi/ https://doi.org/10.1021/acs.macromol.2c02130
105. M. Zaman, A. Iqbal, H.S. Sarwar, M.H. Butt, M.O. Iqbal, N. Nissar, A. Mumtaz, H.Y. Nazzer, A. Alshammari, M.S. Riaz, Application of nanoprecipitation technique to develop poloxamer-407 facilitated solid lipid nanoparticles for the controlled delivery of tacrolimus. Int. J. Polym. Sci. **2023**, 7356899 (2023). https://doi.org/10.1155/2023/7356899
106. M.S. El-Aasser, W. Roy, Tess Award. J. Coat. Technol. Res. **1**, 20–31 (2004). https://doi.org/10.1007/s11998-004-0021-3
107. A. Dolan, J.M. de la Perrelle, T.D. Small, E.R. Milsom, G.F. Metha, X. Pan, M.R. Andersson, D.M. Huang, T.W. Kee, Surfactant effects on hydrogen evolution by small-molecule nonfullerene acceptor nanoparticles. ACS Appl. Nano Mater. **5**, 12154–12164 (2022). https://pubs.acs.org/doi/ https://doi.org/10.1021/acsanm.2c02350
108. J. Kosco, M. Bidwell, H. Cha, T. Martin, C.T. Howells, M. Sachs, D.H. Anjum, S.G. Lopez, L. Zou, A. Wadsworth, W. Zhang, L. Zhang, J. Tellam, R. Sougrat, F. Laquai, D.M. De Longchamp, J.R. Durrant, I. McCulloch, Enhanced photocatalytic hydrogen evolution from organic semiconductor heterojunction nanoparticles. Nat. Mater. **19**, 559–565 (2020). https://doi.org/10.1038/s41563-019-0591-1
109. M.H. Elsayed, M. Abdellah, A.Z. Alhakemy, I.M.A. Mekhemer, A.E.A. Aboubakr, B.H. Chen, A. Sabbah, K.H. Lin, W.S. Chiu, S.J. Lin, C.Y. Chu, C.H. Lu, S.D. Yang, M.G. Mohamed, S.W. Kuo, C.H. Hung, L.C. Chen, K.H. Chen, H.H. Chou, Overcoming small-bandgap charge recombination in visible and NIR-light-driven hydrogen evolution by engineering the polymer photocatalyst structure. Nat. Commun. **15**, 707 (2024). https://doi.org/10.1038/s41467-024-45085-6
110. W.C. Lin, Y.E. Sun, Y.R. Zhuang, T.F. Huang, K.J. Lin, M.M. Elsenety, J.C. Yen, H.K. Hsu, B.H. Chen, C.Y. Chang, J.W. Chang, H.N. Huang, B.H. Li, S. Jungsuttiwong, T. Haldar, S.H. Wang, W.C. Lin, T.L. Wu, C.W. Chen, C.H. Yu, A.C. Su, K.H. Lin, U.S. Jeng, S.D. Yang, HH Chou, optimally miscible polymer bulk-heterojunction-particles for nonsurfactant photocatalytic hydrogen evolution. J. Am. Chem. Soc. **147**, 2537–2548 (2025). https://doi.org/10.1021/jacs.4c13856
111. J. Bruder, K. Fischer, J. Armleder, E. Müller, N.D. Roit, S. Behrens, Y. Peng, W. Wenzel, H. Röhm, A. Colsmann, Photocatalytic hydrogen generation in surfactant-free, aqueous organic nanoparticle dispersions. Small **20**, 2406236 (2024). https://doi.org/10.1002/smll.202406236
112. S.D. Andure, N. Tiwari, Review on UV visible spectroscopic technique. Int. J. Pharm. Res. Appl. **7**, 1288–1299 (2022). https://doi.org/10.35629/7781-0706863868
113. J. Liqiang, Q. Yichun, W. Baiqi, L. Shudan, J. Baojiang, Y. Libin, F. Wei, F. Honggang, S. Jiazhong, Review of photoluminescence performance of nano-sized semiconductor materials and its relationships with photocatalytic activity. Sol Energy Mater. Sol Cells **90**, 1773–1787 (2006). https://doi.org/10.1016/j.solmat.2005.11.007
114. K. Kanemoto, T. Sudo, I. Akai, H. Hashimoto, T. Karasawa, Y. Aso, T. Otsubo, Intrachain photoluminescence properties of conjugated polymers as revealed by long oligothiophenes and polythiophenes diluted in an inactive solid matrix. Phys. Rev. B **73**, 235203 (2006). https://doi.org/10.1103/PhysRevB.73.235203
115. T. Han, X. Wang, D. Wang, B.Z. Tang, Functional polymer systems with aggregation-induced emission and stimuli responses. Top. Curr. Chem. **379**, 7 (2021). https://doi.org/10.1007/s41061-020-00321-7
116. J. Wang, D. Wang, E.K. Miller, D. Moses, G.C. Bazan, A.J. Heeger, Photoluminescence of water-soluble conjugated polymers: origin of enhanced quenching by charge transfer. Macromolecules **33**, 5153–5158 (2000). https://pubs.acs.org/doi/ https://doi.org/10.1021/ma000081j
117. B. Li, L. Ren, D. Jiang, M. Jia, M. Zhang, G. Xu, Y. Sun, L. Hou, C. Yuan, Y. Yuan, Optimizing charge carrier dynamics in photocatalysts for enhanced $CO_2$ photoreduction: fundamental principles, advanced strategies, and characterization techniques. Next Energy **7**, 100222 (2025). https://doi.org/10.1016/j.nxener.2024.100222

118. Y. Tamai, Y. Murata, S. Natsuda, Y. Sakamoto, How to interpret transient absorption data? An overview of case studies for application to organic solar cells. Adv. Energy Mater. **14**, 2301890 (2023). https://doi.org/10.1002/aenm.202301890
119. Y. Wang, P. Maity, Y. Jia, B. Liu, L. Zhao, Y. Li, W. Li, Z. Fei, M. Heeney, S.P. Nunes, W.L. Li, O.F. Mohammed, H. Zhang, Intrinsically charge-generating polymers with long-lived free carriers for efficient photon-to-hydrogen conversion. Sci. Adv. **11**, eaea4191 (2025). https://doi.org/10.1126/sciadv.aea4191
120. G. Boschloo, A. Hagfeldt, Photoinduced absorption spectroscopy as a tool in the study of dye-sensitized solar cells. Inorg. Chim. Acta **361**, 729–734 (2008). https://doi.org/10.1016/j.ica.2007.05.040
121. J. Johnston, C. O'Rourke, A. Mills, Photoinduced absorption spectroscopy (PIAS) study of water and chloride oxidation by a $WO_3$ photoanode in acidic solution. Phys. Chem. Chem. Phys. **25**, 31825–31835 (2023). https://doi.org/10.1039/D3CP03167E
122. T.H. Lee, S.A.J. Hillman, S. Gonzalez-Carrero, A. Difilippo, J.R. Durrant, Long-lived charges in Y6:PM6 bulk-heterojunction photoanodes with a polymer overlayer improve photoelectrocatalytic performance. Adv. Energy Mater. **13**, 2300400 (2023). https://doi.org/10.1002/aenm.202300400
123. A.A. Wilson, T.P. Shalvey, A. Kafizas, A. Mumtaz, J.R. Durrant, Analysis of charge trapping and long lived hole generation in $SrTiO_3$ photoanodes. Sustain. Energy Fuels **7**, 5066–5075 (2023). https://doi.org/10.1039/D3SE00886J
124. G. Magdy, E. Aboelkassim, S.M. Abd Elhaleem, F. Belal, A comprehensive review on silver nanoparticles: synthesis approaches, characterization techniques, and recent pharmaceutical, environmental, and antimicrobial applications. Microchem. J. **196**, 109615 (2024). https://doi.org/10.1016/j.microc.2023.109615
125. S. Wu, Z. Zhang, Y. Lee, Y. Li, X. Tai, W. Si, S. Bai, Y. Lin, Reversing surface charge for highly-active organic photovoltaic catalysts. Angew Chem. Int. Ed. **64**, e202422779 (2024). https://doi.org/10.1002/anie.202422779
126. A. Caglar, T.A. Hansu, H. Demir-Kivark, in *Carbon-Based Metal Free Catalysts*, ed. A.M.A. Asiri, A. Khan, S.A. Bhawani, B.M.M. Abu-zied, S. Siengchin, H. Džudžević-čančar (Elsevier, Amsterdam 2022), p. 127. https://doi.org/10.1016/B978-0-323-88515-7.00005-5
127. C.L. Chang, W.C. Lin,L.Y. Ting, C.H. Shih, S.Y. Chen, T.F. Huang, H. Tateno,J. Jayakumar, W.Y. Jao, C.W. Tai, C.Y. Chu, C.W. Chen, C.H. Yu, Y.J. Lu, C.C. Hu, A.M. Elewa, T. Mochizuki, H.H.Chou, Main-chain engineering of polymer photocatalysts with hydrophilic non-conjugated segments for visible-light-driven hydrogen evolution. Nat. Commun. **13**, 5460 (2022). https://doi.org/10.1038/s41467-022-33211-1
128. J. Alvarez, G. Saudino, V. Musteata, P. Madhavan, A. Genovese, A.R. Behzad, R. Sougrat, C. Boi, K.V. Peinemann, S.P. Nunes, 3D analysis of ordered porous polymeric particles using complementary electron microscopy methods. Sci. Rep. **9**, 13987 (2019). https://doi.org/10.1038/s41598-019-50338-2
129. W. Zhao, L. Luo, M. Cong, X. Liu, Z. Zhang, M. Bahri, B. Li, J. Yang, M. Yu, L. Liu, Y. Xia, N.D. Browning, W.H. Zhu, W. Zhang, A.I. Cooper, Nanoscale covalent organic frameworks for enhanced photocatalytic hydrogen production. Nat. Commun. **15**, 6482 (2024). https://doi.org/10.1038/s41467-024-50839-3
130. H. Gong, Y. Xing, J. Li, S. Liu, Functionalized linear conjugated polymer/$TiO_2$ heterojunctions for significantly enhancing photocatalytic $H_2$ evolution. Molecules **29**, 1103 (2024). https://doi.org/10.3390/molecules29051103
131. S. An, K.J. Jeong, S.Z. Hassan, G. Ham, S. Kang, J. Lee, H. Ma, J. Kwon, S.Y. Jeong, J. Yang, H.Y. Woo, H.H. Cho, H. Cha, C.Y. Son, D.S. Chung, Hydrophilic photocrosslinkers as a universal solution to endow water affinity to a polymer photocatalyst for an enhanced hydrogen evolution rate. Adv. Sci. **11**, 2309786 (2024). https://doi.org/10.1002/advs.202309786
132. Y. Mao, Y. Su, B.S. Hsiao, Probing structure and orientation in polymers using synchrotron small- and wide-angle X-ray scattering techniques. Eur. Polym. J. **81**, 433–446 (2016). https://doi.org/10.1016/j.eurpolymj.2016.01.032
133. J.H. Jhaveri, Z.V.P. Murthy, A comprehensive review on anti-fouling nanocomposite membranes for pressure driven membrane separation processes. Desalination **379**, 137–154 (2016). https://doi.org/10.1016/j.desal.2015.11.009
134. X. Wang, B. Chen, W. Dong, X. Zhang, Z. Li, Y. Xiang, H. Chen, Hydrophilicity-Controlled conjugated microporous polymers for enhanced visible-light-driven photocatalytic $H_2$ evolution. Macromol. Rapid Commun. **40**, 1800494 (2018). https://doi.org/10.1002/marc.201800494
135. D.N.G. Krishna, J. Philip, Review on surface-characterization applications of X-ray photoelectron spectroscopy (XPS): recent developments and challenges. Appl. Surf. Sci. Adv. **12**, 100332 (2022). https://doi.org/10.1016/j.apsadv.2022.100332
136. J. Kim, J.P. Jeon, Y.H. Kim, N.T.D. Anh, K. Chung, J.M. Seo, J.B. Baek, Simple functionalization of a donor monomer to enhance charge transfer in porous polymer networks for photocatalytic hydrogen evolution. Angew Chem. Int. Ed. **63**, e202319395 (2024). https://doi.org/10.1002/anie.202319395
137. Y. Bai, C. Li, L. Liu, Y. Yamaguchi, M. Bahri, H. Yang, A. Gardner, M.A. Zwijnenburg, N.D. Browning, A.J. Cowan, A. Kudo, A.I. Cooper, R.S. Sprick, Photocatalytic overall water splitting under visible light enabled by a particulate conjugated polymer loaded with palladium and iridium. Angew Chem. Int. Ed. **61**, e202201299 (2022). https://doi.org/10.1002/anie.202201299
138. Y. Bai, L. Willbraham, B.J. Slater, M.A. Zwijnenburg, R.S. Sprick, A.I. Cooper, Accelerated discovery of organic polymer photocatalysts for hydrogen evolution from water through the integration of experiment and theory. J. Am. Chem. Soc. **141**, 9063–9071 (2019). https://pubs.acs.org/doi/ https://doi.org/10.1021/jacs.9b03591
139. R.J. Lyons, Y. Yang, E. McQueen, L. Luo, A.I. Cooper, M.A. Zwijnenburg, R.S. Sprick, Polymer photocatalysts with side chain induced planarity for increased activity for sacrificial hydrogen production from water. Adv. Energy Mater. **14**, 2303680 (2024). https://doi.org/10.1002/aenm.202303680
140. T. Banerjee, F. Podjaski, J. Kroger, B.P. Biswal, B.V. Lotsch, Polymer photocatalysts for solar-to-chemical energy conversion. Nat. Rev. Mater. **6**, 168 (2021). https://doi.org/10.1038/s41578-020-00254-z
141. D.C. Coffey, B.W. Larson, A.W. Hains, J.B. Whitaker, N. Kopidakis, O.V. Boltalina, S.H. Strauss, G. Rumbles, An optimal driving force for converting excitons into free carriers in excitonic solar cells. J. Phys. Chem. C **116**, 8916–8923 (2012). https://pubs.acs.org/doi/ https://doi.org/10.1021/jp302275z
142. H. Yan, M. Shen, Y. Shen, G. Ouyang, Spontaneous exciton dissociation in organic photocatalyst under ambient conditions for highly efficient synthesis of hydrogen peroxide. Proc. Natl. Acad. Sci. USA **119**, e2202913119 (2022). https://doi.org/10.1073/pnas.2202913119
143. K. Bai, X. Yu, G. Wen, Y. Yang, Y. Lin, L. Zhang, J. Rong, L.C. Yin, W. Qi, M. Bonn, H.I. Wang, G. Liu, Spontaneous dissociation of excitons in polymeric photocatalysts for overall water splitting. Nat. Commun. **16**, 8577 (2025). https://doi.org/10.1038/s41467-025-63590-0
144. J. Kosco, S. Gonzalez-Carrero, C.T. Howells, W. Zhang, M. Moser, R. Sheelamanthula, L. Zhao, B. Willner, T.C. Hidalgo, H. Faber, B. Purushothaman, M. Sachs, H. Cha, R. Sougrat, T.D. Anthopoulos, S. Inal, J.R. Durrant, I. McCulloch, oligoethylene glycol side chains increase charge generation in organic semiconductor nanoparticles for enhanced photocatalytic hydrogen evolution. Adv. Mater. **34**, 2105007 (2021). https://doi.org/10.1002/adma.202105007
145. Y. Li, Y. Wu, D. Wang, X. Zhang, T. Xiao, J. Zheng, G. Zhang, Simultaneously suppressing non-radiative and radiative recombination of linear conjugated polymer photocatalysts for boosting visible/near-infrared light photocatalytic hydrogen production. Appl. Catal. B **382**, 125960 (2026). https://doi.org/10.1016/j.apcatb.2025.125960
146. S. Giannini, J. Blumberger, Charge transport in organic semiconductors: the perspective from nonadiabatic molecular dynamics. Acc. Chem. Res. **55**, 819–830 (2022). https://pubs.acs.org/doi/ https://doi.org/10.1021/acs.accounts.1c00675
147. S. An, Z. Wu, H. Jeong, J. Lee, S.Y. Jeong, W. Lee, S. Kim, J.W. Han, J. Lim, H. Cha, H.Y. Woo, D.S. Chung, Synergistic contribution of Oligo(ethylene glycol) and fluorine substitution of conjugated polymer photocatalysts toward solar driven sacrificial hydrogen evolution. Small **19**, 2204905 (2022). https://doi.org/10.1002/smll.202204905
148. C.M. Pelicano, H. Tong, Recent advances in cocatalyst engineering for solar-driven overall water splitting. Appl. Res. **3**, e202300080 (2023). https://doi.org/10.1002/appl.202300080
149. Y. Liang, T. Li, Y. Lee, Z. Zhang, Y. Li, W. Si, Z. Liu, C. Zhang, Y. Qiao, S. Bai, Y. Lin, Organic photovoltaic catalyst with σ-π anchor for high-performance solar hydrogen evolution. Angew Chem. Int. Ed. **62**, e202217989 (2023). https://doi.org/10.1002/anie.202217989
150. Y. Abghoui, Superiority of the (100) over the (111) facets of the nitrides for hydrogen evolution reaction. Top. Catal. **65**, 262–269 (2022). https://doi.org/10.1007/s11244-021-01474-5
151. K. He, E. Campbell, Z. Huang, R. Shen, Q. Li, S. Zhang, Y.L. Zhong, P. Zhang, X. Li, Metal carbide-based cocatalysts for photocatalytic solar-to-fuel conversion. Small Struct. **3**, 2200104 (2022). https://doi.org/10.1002/sstr.202200104
152. X. Huang, J. Song, G. Wu, Z. Miao, Y. Song, Z. Mo, Recent progress on the photocatalytic hydrogen evolution reaction over a metal sulfide cocatalyst-mediated carbon nitride system. Inorg. Chem. Front. **11**, 2527–2552 (2024). https://doi.org/10.1039/D4QI00255E
153. W. Ren, J. Wang, X. Zheng, J. Ge, S. Meng, Y. Yang, S. Chen, Transition metal phosphides ($Fe_2P$, $Co_2P$, and $Ni_2P$) modified cds nanorods for efficient photocatalytic $H_2$ evolution. ACS Appl. Nano Mater. **7**, 22137–22146 (2024). https://pubs.acs.org https://doi.org/10.1021/acsanm.4c04156

154. T. Zhang, S. Lu, Sacrificial agents for photocatalytic hydrogen production: effects, cost, and development. Chem. Catal. **2**, 1502–1505 (2022). https://doi.org/10.1016/j.checat.2022.06.023
155. M. Wang, S. Shen, L. Li, Z. Tang, J. Yang, Effects of sacrificial reagents on photocatalytic hydrogen evolution over different photocatalysts. J. Mater. Sci. **52**, 5155–5164 (2017). https://doi.org/10.1007/s10853-017-0752-z
156. M.R.K. Estahbanati, N. Mahinpey, M. Feilizadeh, F. Attar, M.C. Iliuta, Kinetic study of the effects of pH on the photocatalytic hydrogen production from alcohols. Int. J. Hydrog. Energy **44**, 32030 (2019). https://doi.org/10.1016/j.ijhydene.2019.10.114
157. W. Yue, Z. Ye, C. Liu, Z. Xu, L. Wang, X. Cao, H. Yamashita, J. Zhang, Enhanced photocatalytic hydrogen evolution activity driven by the synergy between surface vacancies and cocatalysts: surface reaction matters. Adv. Sci. **11**, 2407092 (2024). https://doi.org/10.1002/advs.202407092
158. M.C.N. Martínez, O. Cavdar, Ł.P. Haliński, M. Miodyńska, P. Parnicka, B. Bajorowicz, M. Kobylański, Ł. Lewandowski, A. Zaleska-Medynska, Hydrogen detection during photocatalytic water splitting: a tutorial. Int. J. Hydrog. Energy **47**, 15783–15788 (2022). https://doi.org/10.1016/j.ijhydene.2022.03.050
159. V. Dippold, H. Küçükkeçeci, E. Bosler, J. Schmidt, S. Ghosh, G. Michi, I.E. Khalil, L. Gerland, A. Lange, D. Oberschmidt, A. Thomas, Carbazole-based thin microporous polymer films for photocatalytic hydrogen evolution. Adv. Mater. **37**, 2506689 (2025). https://doi.org/10.1002/adma.202506689
160. V.L. Pachapur, S.J. Sarma, S.K. Brar, Y.L. Bihan, G. Buelna, M. Verma, Hydrogen production from biodiesel industry waste by using a co-culture of enterobacter aerogenes and *Clostridium butyricum*. Biofuels **8**, 651–662 (2016). https://doi.org/10.1080/17597269.2015.1122471
161. B. Abhishek, A. Jayarama, A.S. Rao, S.S. Nagarkar, A. Dutta, S.P. Duttagupta, S.S. Prabhu, R. Pinto, Challenges in photocatalytic hydrogen evolution: importance of photocatalysts and photocatalytic reactors. Int. J. Hydrog. Energy **81**, 1442–1466 (2024). https://doi.org/10.1016/j.ijhydene.2024.07.262
162. R. Ricka, M. Přibyl, K. Kočí, Apparent quantum yield–key role of spatial distribution of irradiation. Appl. Catal. Gen. **658**, 119166 (2023). https://doi.org/10.1016/j.apcata.2023.119166
163. R. Sayago-Carro, L.J. Jiménez-Chavarriga, E. Fernández-García, A. Kubacka, M. Fernández-García, Efficiency in photocatalytic production of hydrogen: energetic and sustainability implications. Energy Adv. **3**, 2738–2757 (2024). https://doi.org/10.1039/D4YA00361F
164. X. Chen, R. Shi, Q. Chen, Z. Zhang, W. Jiang, Y. Zhu, T. Zhang, Three-dimensional porous g-$C_3N_4$ for highly efficient photocatalytic overall water splitting. Nano Energy **59**, 644–650 (2019). https://doi.org/10.1016/j.nanoen.2019.03.010
165. P. Zhou, I.A. Navid, Y. Ma, Y. Xiao, P. Wang, Z. Ye, B. Zhou, K. Sun, Z. Mi, Solar-to-hydrogen efficiency of more than 9% in photocatalytic water splitting. Nature **613**, 66–70 (2023). https://doi.org/10.1038/s41586-022-05399-1
166. C.F. Fu, J. Sun, Q. Luo, X. Li, W. Hu, J. Yang, Intrinsic electric fields in two-dimensional materials boost the solar-to-hydrogen efficiency for photocatalytic water splitting. Nano Lett. **18**, 6312–6317 (2018). https://pubs.acs.org/doi/ https://doi.org/10.1021/acs.nanolett.8b02561
167. S.B. Beli, S. Bonnet, C. Casadevall, R.J. Detz, F. Eisenreich, S.D. Glover, C. Kerzig, L. Næsborg, S. Pullen, G. Storch, N. Wei, C. Zeymer, Challenges and future perspectives in photocatalysis: conclusions from an interdisciplinary workshop. JACS Au **4**, 2746–2766 (2024). https://pubs.acs.org https://doi.org/10.1021/jacsau.4c00527
168. S. Cañellas, M. Nuño, E. Speckmeier, Improving reproducibility of photocatalytic reactions—how to facilitate broad application of new methods. Nat. Commun. **15**, 307 (2024). https://doi.org/10.1038/s41467-023-44362-0
169. L. Liu, M.A. Kochman, W. Zhao, M.A. Zwijnenburg, R.S. Sprick, Linear conjugated polymer photocatalysts with various linker units for photocatalytic hydrogen evolution from water. Chem. Commun. **58**, 10639–10642 (2022). https://doi.org/10.1039/D2CC03810B
170. H. Zhao, Y. Dong, P. Sun, Y. Bai, C. Ru, X. Wu, Z. Li, X. Han, J. Wu, X. Pan, Effect of D/A ratio on photocatalytic hydrogen evolution performance of conjugated polymer photocatalysts. ACS Appl. Energy Mater. **5**, 4631–4640 (2022). https://pubs.acs.org/doi/ https://doi.org/10.1021/acsaem.2c00017
171. W.C. Lin, C.L. Chang, C.H. Shih, W.C. Lin, Z.Y. Lai, J.W. Chang, L.Y. Ting, T.F. Huang, Y.E. Sun, H.Y. Huang, Y.T. Lin, J.J. Liu, Y.H. Wu, Y.T. Tseng, Y.R. Zhuang, B.H. Li, A.C. Su, C.H. Yu, C.W. Chen, K.H. Lin, U.S. Jeng, H.H. Chou, Sulfide oxidation on ladder-type heteroarenes to construct all-acceptor copolymers for visible-light-driven hydrogen evolution. Small **19**, 2302682 (2023). https://doi.org/10.1002/smll.202302682
172. T.F. Huang, J.J. Liu, Z.Y. Lai, J.W. Chang, Y.R. Zhuang, Z.C. Jiang, C.L. Chang, W.C. Lin, Y.H. Chen, Y.H. Wu, Y.E. Sun, T.A. Luo, Y.K. Chen, J.C. Yen, H.K. Hsu, B.H. Chen, L.Y. Ting, C.Y. Lu, Y.T. Lin, L.Y. Hsu, T.L. Wu, S.D. Yang, A.C. Su, U.S. Jeng, HH Chou, performance and solution structures of side-chain-bridged oligo (ethylene glycol) polymer photocatalysts for enhanced hydrogen evolution under natural light illumination. Small **20**, 2304743 (2023). https://doi.org/10.1002/smll.202304743
173. T.F. Huang, Y.R. Zhuang, C.L. Chang, C.L. Huang, W.C. Lin, Z.C. Jiang, L.Y. Ting, I.M.A. Mekhemer, Y.E. Sun, P. Kidkhunthod, J.L. Chen, Y.C. Huang, H.K. Hsu, Y.T. Tseng, Y.H. Wu, B.H. Li, S.D. Yang, Y.J. Cheng, H.H. Chou, Indanone-based conjugated polymers enabling ultrafast electron transfer for visible light-driven hydrogen evolution from water. J. Mater. Chem. A **12**, 3633–3643 (2024). https://doi.org/10.1039/D3TA06807B
174. X. Xu, J. Liu, Y. Sun, Z. Li, Molecular engineering of novel D–$A_1$–$A_2$ conjugated microporous polymers by efficient electron donor for highly enhanced photocatalytic hydrogen generation. Sep. Purif. Technol. **364**, 132454 (2025). https://doi.org/10.1016/j.seppur.2025.132454
175. M.A. Jr. Melo, Z. Wu, B.A. Nail, A.T.D. Denko, A.F. Nogueira, F.E. Osterloh, Surface photovoltage measurements on a particle tandem photocatalyst for overall water splitting. Nano Lett. **18**, 805–810 (2018). https://pubs.acs.org/doi/ https://doi.org/10.1021/acs.nanolett.7b04020
176. Y. Yang, D. Li, P. Wang, X. Zhang, H. Zhang, B. Du, C. Guo, T. Wang, D. Liu, Polymer/non-fullerene acceptor bulk heterojunction nanoparticles for efficient photocatalytic hydrogen production from water. Polymer **244**, 124667 (2022). https://doi.org/10.1016/j.polymer.2022.124667
177. Z. Zhang, W. Si, B. Wu, W. Wang, Y. Li, W. Ma, Y. Lin, Two-Dimensional polycyclic photovoltaic molecule with low trap density for high-performance photocatalytic hydrogen evolution. Angew Chem. Int. Ed. **61**, e202114234 (2021). https://doi.org/10.1002/anie.202114234
178. X. Liu, Y. Zhao, Y. Ni, F. Shi, X. Guo, C. Li, Hydroxylated organic semiconductors for efficient photovoltaics and photocatalytic hydrogen evolution. Energy Environ. Sci. **16**, 4065–4072 (2023). https://doi.org/10.1039/D3EE00835E
179. Z. Zhang, C. Xu, Q. Sun, Y. Zhu, W. Yan, G. Cai, Y. Li, W. Si, X. Lu, W. Xu, Y. Yang, Y. Lin, Delocalizing excitation for highly-active organic photovoltaic catalysts. Angew Chem. Int. Ed. **63**, e202402343 (2024). https://doi.org/10.1002/anie.202402343
180. L. Shi, A. Troisi, High-throughput screening of molecule/polymer photocatalysts for the hydrogen evolution reaction. ACS Catal. **15**, 6690–6701 (2025). https://pubs.acs.org/doi/ https://doi.org/10.1021/acscatal.5c01785
181. W. Zhang, M. Yu, T. Liu, M. Cong, X. Liu, H. Yang, Y. Bai, Q. Zhu, S. Zhang, H. Gu, X. Wu, Z. Zhang, Y. Wu, H. Tian, X. Li, W.H. Zhu, A.I. Cooper, Accelerated discovery of molecular nanojunction photocatalysts for hydrogen evolution by using automated screening and flow synthesis. Nat. Synth. **3**, 595 (2024). https://doi.org/10.1038/s44160-024-00494-9
182. X. Li, P.M. Maffettone, Y. Che, T. Liu, L. Chen, A.I. Cooper, Combining machine learning and high-throughput experimentation to discover photocatalytically active organic molecules. Chem. Sci. **12**, 10742–10754 (2021). https://doi.org/10.1039/D1SC02150H
183. H.I. Hamoud, L. Wolski, I. Pankin, In situ and *Operando* spectroscopies in photocatalysis: powerful techniques for a better understanding of the performance and the reaction mechanism. Top. Curr. Chem. **380**, 37 (2022). https://doi.org/10.1007/s41061-022-00387-5
184. C. Bie, L. Wang, J. Yu, Challenges for photocatalytic overall water splitting. Chem **8**, 1567–1574 (2022). https://doi.org/10.1016/j.chempr.2022.04.013
185. M. Rahman, H. Tian, T. Edvinsson, Revisiting the limiting factors for overall water-splitting on organic photocatalysts. Angew Chem. Int. Ed. **59**, 16278 (2020). https://doi.org/10.1002/anie.202002561
186. A. Ghosh, A. Pramanik, S. Pal, P. Sarkar, Emergence of Z-scheme photocatalysis for total water splitting: an improvised route to high efficiency. J. Phys. Chem. Lett. **15**, 6841–6851 (2024). https://pubs.acs.org/doi/ https://doi.org/10.1021/acs.jpclett.4c01162
187. M. Yu, W. Zhang, Z. Guo, Y. Wu, W. Zhu, Engineering nanoparticulate organic photocatalysts via a scalable flash nanoprecipitation process for efficient hydrogen production. Angew Chem. Int. Ed. **60**, 15590–15597 (2021). https://doi.org/10.1002/anie.202104233


## Publisher's note